MS ID#: NUTRITION/2017/256164

Folate deficiency facilitates genomic integration of Human Papillomavirus type 16 (HPV16) DNA *in vivo* in a novel mouse model for rapid oncogenic transformation of human keratinocytes[1,2*]

Suhong Xiao[3,4], Ying-Sheng Tang[3,4], Praveen Kusumanchi[5], Sally P. Stabler[6], Ying Zhang[7] and Aśok C. Antony[3,5]

Department of Medicine, Indiana University School of Medicine, Indianapolis, Indiana 46202; Department of Medicine, University of Colorado Anschutz Medical Campus, Aurora, Colorado 80045; Department of Biostatistics, Indiana University Fairbanks School of Public Health, Indianapolis, Indiana 46202; Richard L. Roudebush Veterans Affairs Medical Center, Indianapolis, Indiana 46202.

Last Names and Initials for PubMed indexing:

Xiao S, Tang YS, Kusumanchi P, Stabler SP, Zhang Y, and Antony AC.

Word count of Manuscript: Abstract *plus* Main Text = 7428 words
(References 81)

Number of Figures: 4

Number of Tables: 1

Running Title: Folate nutrition, HPV16 integration, and cancer

[1] Supported by a Veterans Affairs Merit Review Award (to ACA)
[2] All authors declare they have no conflicts of interest with the contents of this article.
[3] Department of Medicine, Indiana University School of Medicine, Indianapolis, Indiana 46202
[4] These authors contributed equally to this work
[5] Richard L. Roudebush Veterans Affairs Medical Center, Indianapolis, Indiana 46202
[6] Department of Medicine, University of Colorado Anschutz Medical Campus, Aurora, Colorado 80045
[7] Department of Biostatistics, Indiana University Fairbanks School of Public Health, Indianapolis, Indiana, 46202
[8] Abbreviations used: AIDS, acquired immunodeficiency syndrome; CIN, cervical intraepithelial neoplasia; DMEM, Dulbecco's Modified Eagles Medium; D-PBS, Dulbecco's phosphate-buffered saline; FBS, Fetal Bovine Serum; GAPDH, glyceraldehyde-3-phosphate dehydrogenase; GST, glutathione *S*-transferase; hnRNP-E1, heterogeneous nuclear ribonucleoprotein E1; -HF, high-folate; HIV, human immunodeficiency virus; HPV16, Human Papillomavirus Type 16; -LF, low-folate; nt, nucleotide; qRT-PCR, quantitative real-time reverse-transcriptase polymerase chain reaction. 5'-UTR, 5'-untranslated region.
* To whom correspondence should be addressed. Email: aantony@iu.edu or 980 West Walnut Street, R3 C321B, Indianapolis, Indiana 46202.

Abstract

Background: Epidemiological and *in vitro* studies suggest independent linkages between poor folate-and/or-vitamin-B_{12} nutrition, genomic HPV16-viral integration, and cancer. However, there is no direct evidence *in vivo* to support the causative role of poor-folate nutrition in HPV16-integration into the cellular genome.

Objective: We tested the hypothesis that folate deficiency was permissive for the integration of HPV16 into the genome of HPV16-harboring keratinocytes, and could thereby influence earlier transformation of these cells to cancer in an animal model.

Methods: HPV16-harboring human keratinocytes [(HPV16)BC-1-Ep/SL] were differentiated into 3-Dimensional HPV16-organotypic rafts under either folate-replete or folate-deficient conditions *in vitro.* These were then subcutaneously implanted in severely immunocompromised 4-6-week old, 16-18-gm female, Beige Nude XID (Hsd:NIHS-*Lyst*^{bg}*Foxn1*^{nu}*Btk*^{xid}) mice fed either a folate-replete diet (1200-nmol folate/kg diet) or progressively folate-deficient diet (600- or 400-nmol/kg diet, respectively) for 2-months prior to raft-implantation surgery, and indefinitely thereafter. The tumors that subsequently developed were characterized for onset, pattern of growth, morphology, HPV16-oncogene expression, and HPV16-genomic integration.

Results: All HPV16-organotypic rafts developed in either folate-replete or physiological low-folate media *in vitro* and subsequently implanted in folate-replete mice eventually transformed into aggressive malignancies within weeks. When compared to HPV16-*high folate*-organotypic raft-derived tumors from mice fed either a 1200- or 600-nmol folate/kg diet, those raft-derived cancers that developed in mice fed a 400-nmol folate/kg diet *a)* expressed significantly more HPV16 E6 (1.8-fold more) and E7 (2.8-fold more) oncogenic proteins ($P = 0.001$), and *b)* revealed significantly more HPV16-integration sites in genomic DNA (2-fold more), either directly into, or in the vicinity of, cellular genes ($P < 0.05$).

Conclusions: This unprecedented animal model for the consistent rapid transformation of differentiated (HPV16)BC-1-Ep/SL-derived organotypic raft-keratinocytes to cancer in Beige Nude XID mice confirms that dietary folate deficiency can profoundly influence and modulate events leading to HPV16-induced carcinogenesis, and facilitates genomic integration of HPV16 DNA *in vivo*.

Keywords: Human papillomavirus type 16; cancer; oncogenes; folate/vitamin-B_{12} nutrition; organotypic rafts; genomic integration; immunodeficiency; mouse model

Introduction

Human papillomavirus type 16 (HPV16)[7] is globally responsible for an estimated one-half of all HPV-associated genital and oropharyngeal cancers worldwide (1). Apart from repeated exposure to HPV16-infected material, or inability to eradicate the virus among individuals with immunodeficiency states, most short-term exposures to HPV16-infections remain transient and are cleared within 2 years. And, although there can be long term viral persistence in less than 10% of new infections, an even smaller number of such cases will progress to precancerous lesions and cancer in immunocompetent individuals over a time frame that is usually well beyond a decade (2). Integration of HPV16 DNA into the host genome, which converts the circular episomal DNA into a linear truncated DNA wherein both HPV16 E6/E7 oncogenes are intact (3, 4) and HPV16 E2-mediated repression of E6/E7 is lost (5), is an important reason for persistence of HPV, and can be a critical event in carcinogenesis and survival (6-10). Thus, in HPV18-induced cancers, the prevalence of integrated sequences approaches 100% (9, 11); however, in the case of HPV16, pathways arising from *both* genomic integration and the presence of HPV16 DNA episomes can induce cancer (9, 12, 13).

On the basis of epidemiological data, established co-factors that accelerate HPV-induced transformation of tissues to cancer include early age at first intercourse, multiple partners, smoking, oral contraceptives, and reduced immunity arising from advanced human immunodeficiency virus (HIV) infection and acquired immunodeficiency syndrome (AIDS), or primary immunodeficiency states (14). Poor folate-and/or-vitamin-B_{12} nutrition, which is common worldwide (15-17), has been suspected as a co-factor for HPV-induced cancers for 3 decades (18-23). Thus, *a)* both experimental and clinical folate- and vitamin-B_{12}- deficiency, predisposes to fragmentation of DNA (24-28), and induces breaks within both common- and

rare- fragile sites in DNA (29-32), resulting in genomic instability. *b)* Further documentation of the coincidence of HPV16 viral integration into common and rare fragile sites, and the finding of preferential HPV16 integration in common fragile sites within (HPV16-induced) cervical tumors raised the possibility that HPV16 DNA integration can trigger oncogenesis through insertional mutagenesis of tumor suppressor genes (29-35). *c)* Confirmation of several such genes within common fragile sites lent further biological plausibility to the potential for folate/vitamin-B_{12}-deficiency, HPV16 integration, and cancer, to be linked. However, neither direct experimental studies *in vivo* nor clinical studies have definitively demonstrated that the folate- or vitamin-B_{12}-deficient state *per se* is permissive for an increase in integration of HPV16 into genomic DNA. Earlier we determined another molecular mechanism whereby folate deficiency triggers the homocysteinylation and activation of an mRNA-binding protein, hnRNP-E1 (36, 37), which avidly binds HPV16 RNA and profoundly perturbs generation of both HPV16 L1 and L2 viral capsid proteins *in vitro,* in cultured HPV16-harboring BC-1-Ep/SL keratinocyte monolayers, as well as in differentiated 3-Dimensional HPV16-organotypic rafts developed in physiological low-folate medium (38). As a result, when compared to control 18-day HPV16-*high folate*-organotypic rafts (referred to hereafter as HF-rafts), the HPV16-*low folate*-organotypic rafts (referred to hereafter as LF-rafts) contained *a)* much fewer HPV16-viral particles, *b)* a similar HPV16 DNA viral load, but *c)* much greater extent of viral integration of HPV16 DNA into genomic DNA (38). Although these studies unequivocally established a molecular linkage between poor folate-nutrition and an altered HPV16 life cycle *in vitro*, two outstanding questions remained: *i),* When did the high level of integration of HPV16 DNA into the genomic DNA of human keratinocytes occur in LF-rafts that were developed *in vitro? ii),* Did HPV16 DNA also integrate into the genomic DNA of human keratinocytes *in vivo,* and was it more frequent in folate-deficient *versus* folate-replete tissues *in vivo*?

In addition, when 18-day old HF-rafts and LF-rafts were subcutaneously implanted into 3 different species of folate-replete mice with varying degrees of immunodeficiency, only one of two severely immunocompromised Beige Nude XID mice implanted with an LF-raft developed an aggressive cancer at the site of implantation within 12 weeks (38). This raised the obvious question of whether the development of this cancer was a stochastic event. Therefore, it was incumbent on us to clarify the frequency with which our differentiated HPV16-organotypic rafts would develop into cancer in this model using Beige Nude XID mice, which possess no capacity to recognize and eradicate HPV16 viruses because they lack B, T, and NK cells [see Ref. (38), *Supplement Table S1*].

To address these issues, we studied the fate of cultured HPV16-harboring BC-1-Ep/SL cells that were differentiated into HPV16-organotypic rafts under high- or low- folate conditions *in vitro* and then subcutaneously implanted in Beige Nude XID mice that were chronically fed either a folate-replete or progressively folate-deficient diet (38).

Methods

Materials: HPV16 plasmid DNA was a kind gift from Professor Ann Roman (Indiana University). BC-1-Ep/SL keratinocytes that had been stably transfected with HPV16 (39)—referred to hereafter as (HPV16)BC-1-Ep/SL cells—were a kind gift from Professor Paul F. Lambert (University of Wisconsin). NIH/3T3 (ATCC® CRL-1658™) was obtained from American Type Culture Collection (Manassas, VA). An anti-HPV16 E6 + HPV18 E6 mouse monoclonal antibody [clone C1P5] (ab70) (Abcam, Cambridge, MA), which was generated against purified HPV-18 E6-beta galactosidase fusion protein, recognizes E6 from both HPV16 and HPV18; its specificity has been validated previously (40, 41). An anti-HPV E7 mouse

monoclonal antibody [289-17013] which was generated against the full length HPV16 E7 protein (Abcam, Cambridge, MA), is specific for HPV16 E7 protein as validated previously (42, 43).

Animal Protocols and Animal Care. All animal care procedures conformed to the "Guide for the Care and Use of Laboratory Animals" (44). The protocols for the use of Beige Nude XID mice were approved by the Institutional Animal Care & Use Committee at Indiana University-Purdue University at Indianapolis.

Model for the implantation of HPV16-organotypic rafts in mice with defined folate diets. Seventy-two female Beige Nude XID (Hsd:NIHS-*Lyst*^{bg}*Foxn1*^{nu}*Btk*^{xid}), 4-6 week old, and weighing 16-18 grams were obtained from Harlan Sprague Dawley Laboratories, Indianapolis, IN, and acclimatized for one week at the Laboratory Animal Resource Center at Indiana University School of Medicine.

Mice were fed a defined diet (from Dyets Inc, Bethlehem, PA) that contained 1% succinyl sulfathiazole and various concentrations of folic acid for two months (as we described (44)) before implantation of HPV16-organotypic rafts. These diets, detailed in **Supplemental Tables** 1-5, were composed of an optimum [normal] diet of 1200-nmol folate/kg diet (0.529 mg/kg) or either one of two progressively folate-deficient diets (i.e., 600-nmol folate/kg diet (0.265 mg/kg), or 400-nmol folate/kg diet (0.177 mg/kg) (44). [We have earlier determined that by the end of two months on these folate-deficient diets, mice tend to exhibit evidence of folate deficiency, manifested by a reduction in serum folate and an inverse rise in serum homocysteine, which is proportionate to the degree of dietary folate restriction (44)]. After subcutaneous surgical implantation of HPV16-organotypic rafts, each of these mice were then maintained on their pre-implantation diets throughout the observation period of each experiment.

Forty-eight mice were randomly divided equally into three dietary folate groups (either 1200-, or 600-, or 400- nmol folate/kg diet) and housed individually in specialized wire-

bottomed stainless-steel cages (to minimize coprophagy during induction of a dietary folate deficiency) (44). These groups were subcutaneously implanted with HF-rafts. In another experiment, twenty-four mice that were fed a 1200-nmol folate/kg diet were implanted subcutaneously with LF-rafts.

Previous approaches employed to implant fragments of HPV-infected human foreskins under the skin of mice (45, 46), were modified for subcutaneous implantation of either HF-rafts or LF-rafts in Beige Nude XID mice. Briefly, 18-day old HF-rafts and LF-rafts were washed with sterile D-PBS, cut into 5x5x1 mm pieces, and transported in Petri dishes at 4°C to the animal facility in either F-HF or F-LF medium, respectively. [The composition of F-HF and F-LF media is detailed in **Supplemental Methods**].

All mice remained deeply anesthetized before and throughout the surgical procedure as described in **Supplemental Methods.** Under sterile conditions, a 0.5 cm mid-flank skin incision was made perpendicular to the spine below the costophrenic angle with scissors, and a subcutaneous pocket was created using blunt forceps. A fragment (5x5x1 mm) from either a HF-raft or LF-raft was then inserted subcutaneously and repositioned in a top-to-bottom orientation to facilitate angiogenesis of the raft from below, and the incision was closed with a surgical clip. After postoperative recovery from anesthesia, the mouse was transferred to a regular cage. The surgical clips were removed one week after surgery without anesthesia. The mice were then observed twice a week for tumor growth. Once tumors were established, measurements were taken on a regular basis (45, 46). Quantification of tumor growth was made using the formula, as described (47). Mice were euthanized in a CO_2 chamber for 5 minutes followed by cervical dislocation to confirm death.

Although several mice developed subcutaneous cysts at the site of implantation of rafts shortly after the surgical clips were removed, none of these grew over 50 mm^3 before they either

regressed or receded into a minor swelling over the implantation area. Accordingly, the swelling was formally recorded as a tumor only when the tumors grew beyond the 50 mm^3 volume.

To assess the intrinsic malignant potential of (HPV16)BC-1-Ep/SL keratinocytes propagated in high-folate medium, 3 million cells were injected subcutaneously into the flanks of Beige Nude XID mice fed a folate-replete diet. Mice were evaluated for the development of a tumor at the site of injection for up to 38 weeks before being sacrificed.

Tumor RNA preparation and Quantitative Reverse Transcriptase-PCR (qRT-PCR), primers, and validation. Total RNA was extracted from tumor tissue using the GenElute Mammalian Total RNA Miniprep kit and the manufacturer's instructions. Specific primers were designed to amplify HPV16 E6, E7 RNA using the online Integration DNA Technologies software. Primers for HPV16 E6 were as follows: Fluorescent probe: 5'-/56-FAM/AGA ATG TGT/ZEN/GTA CTG CAA GCA ACA GT/31 ABkFQ/-3'; forward primer: 5'-CGA CCC AGA AAG TTA CCA CAT -3'; reverse primer: 5'-AGC AAA GTC ATA TAC CTC ACG TC-3'. Primers for HPV16 E7 were as follows: Fluorescent probe: 5'-/56-FAM/TGC GTA CAA/ZEN/AGC ACA CAC GTA GAC A/31ABkFQ/-3'; forward primer: 5'-TGT TGC AAG TGT GAC TCT ACG -3'; reverse primer: 5'-TGT GCC CAT TAA CAG GTC TTC-3'. Primers for the mouse housekeeping gene, glyceraldehyde-3-phosphate dehydrogenase (GAPDH), were as follows: Fluorescent probe: 5'-/56-JOEN/TCA AGA AGG/ZEN/TGG TGA AGC AGG CAT/31 ABkFQ/-3'; forward primer: 5'-GGA GAA ACC TGC CAA GAT TGA -3'; reverse primer: 5'-TCC TCA GTG TAG CCC AAG A-3'. qRT-PCR was performed on an ABI 7900 Sequence Detection System (PE Biosystems, Foster City, CA) using a SuperScript III Platinum One-Step qRT-PCR kit (Invitrogen, CA). Cycle conditions were as follows: After the first step for 10 min at 50°C and 2 min at 95°C, the samples were cycled 40 times at 95°C for 15 seconds and at 60°C for 60 seconds. For all quantitative analyses the comparative threshold cycle method [or relative

177 standard curve method] was followed according to the PE Biosystems instruction manual. All
178 PCR reactions were performed in duplicate. Primers to mouse GAPDH were run in parallel to
179 standardize the input amount. The extent of densitometry-scanned signals of HPV16 E6 and E7
180 protein expression in each tumor normalized to the amount of β-actin protein loaded onto each
181 gel was first expressed as the percent HPV16 E6/E7/β-actin ratio per tumor (n = 10 per dietary
182 group), and the mean group percent HPV16 E6/E7/β-actin ratio of each dietary group was then
183 assessed for statistical significance.

184 ***Localization of genomic integration of HPV16 by Junction-PCR***. Junction-PCR was conducted
185 on each tumor to detect the genomic integration site in various tumor samples using a panel of 75
186 pairs of primer combinations [shown in Ref. (48), Supplemental Table S7] which were custom-
187 synthesized by Integrated DNA Technologies (Coralville, IA). These 75 primer pairs had
188 previously been defined as loci for integration of HPV16 in genomic DNA from established
189 human cervical cancers (48). Junction-PCR was performed with the High Fidelity PCR Master
190 Kit (Roche). The 20 μL reaction components comprised 10-μL of 2X master mix, 1-μL HPV16
191 forward primer (10-μM), 1-μL cellular primer (10-μM), 1-μL of template DNA (50-ng/μL), and
192 7-μL of PCR-grade water. Cycling conditions were as follows: Initial denaturation/activation at
193 94 °C (5 min), 35 cycles including denaturation at 94 °C (30 sec), annealing at 59 °C (30 sec),
194 and elongation at 72 °C (1 min). PCR products were assessed using Agarose Gel Electrophoresis.

195 ***Supplemental Methods.*** The following experiments can be found in the **Supplemental Methods**
196 (**Online Supporting Materials**): Culture of (HPV16)BC-1-Ep/SL keratinocytes in high-folate F-
197 medium and adaptation to low-folate F-medium in the absence of feeder layers; HPV16-
198 organotypic raft cultures; Quantitative PCR (qPCR) for HPV16 viral load and estimation of

HPV16 DNA integration ratio; Sedation and anesthesia of mice; and Measurement of serum homocysteine in mice.

Statistical analyses. Statistical analysis was conducted using GraphPad Prism 6 (GraphPad Software, San Diego, CA). Unless otherwise specified, results are expressed as means ± SDs, n = 3 (means of triplicates). Comparisons between 2 groups were analyzed by Student's t test and comparison between multiple groups were analyzed using one-way ANOVA followed by a post-hoc multiple comparisons (Tukey's test) if the one-way ANOVA resulted in statistical significance at level 0.05.

Results

Determination of HPV16 DNA integration into the genome in HPV16-harboring cells in vitro. The observed high-level integration of HPV16 DNA into the cellular genome of LF-rafts at day-19 (38) could have occurred either during raft development over 18 days *in vitro,* or at an earlier time. Accordingly, LF-rafts in development were placed back into high-folate (F-HF) medium during various days of culture and the HPV16 DNA integration ratio, which reflected the extent of genomic integration of HPV16 DNA, was reassessed on day-19 (when these rafts were dismantled). As shown in **Figure** 1 A, propagation of LF-rafts after placing back in F-HF medium failed to reverse the extant high-level integration into genomic DNA. These studies pointed to the occurrence of high-level genomic integration of HPV16 DNA at an earlier time when (HPV16)BC-1-Ep/SL cells were adapted to low-folate media.

Immortalized (HPV16)BC-1-Ep/SL keratinocytes propagated as monolayers in culture contain HPV16 DNA episomes. When (HPV16)BC-1-Ep/SL keratinocytes that were stably propagated in F-HF media were abruptly passaged in low-folate (F-LF*)* medium and evaluated over 25 weeks, there was a progressive increase in HPV16 integration into the cellular genome

223 [based on the integration ratio (38)], from a baseline value for integration between 40-45% in F-
224 HF medium to a high of 95% integration into genomic DNA (**Figure** 1 B). Near maximal
225 integration occurred from the 7th week onwards; this was the time when other cells are known to
226 become progressively folate-deficient when similarly propagated in low-folate medium (36, 38).
227 Parenthetically, this is also the period of accumulation of homocysteine intracellularly sufficient
228 to trigger homocysteinylation of hnRNP-E1 (37) leading to translational up-regulation of folate
229 receptors (36). Thus folate deficiency, which is known to favor fragmentation of DNA
230 (discussed in Ref. (38)), was likely to have been permissive for the integration of HPV16 DNA
231 episomes into the genomic DNA of (HPV16)BC-1-Ep/SL cells in culture.

232 ***Characteristics of tumors following transformation of HPV16-organotypic rafts to cancer in***
233 ***Beige Nude XID mice.*** When 3 million (HPV16)BC-1-Ep/SL cells that were propagated in F-HF
234 medium were subcutaneously implanted into the flanks of each of three folate-replete Beige
235 Nude XID mice, no tumor was detected even after 38 weeks of observation. These results
236 indicated that such HPV16-immortalized cells were not intrinsically malignant.

237 Next, we determined the frequency with which subcutaneous implantation of
238 differentiated 18-day old HF-rafts in female Beige Nude XID mice were transformed to cancer.
239 After implantation into three dietary groups of 16 mice each, the majority of mice survived long-
240 term observation; however, in the 1200-, 600-, and 400-nmol folate/kg diet groups, there were 2,
241 4, and 3 mice, respectively, that failed to thrive before development of tumors and were
242 euthanized on the recommendation of the supervising veterinarian.

243 **Supplemental Figure** 1 A-D illustrates various stages in transformation of
244 subcutaneously implanted differentiated HPV16-organotypic rafts into tumors in representative
245 mice. In several mice, there was a small cyst which developed and then either resolved within a
246 couple of weeks or from which a tumor developed. However, in time, once firm nodules

developed, there was usually a rapid tumor doubling time consistent with an aggressive cancer, necessitating early euthanasia of the mouse. On light microscopy these tumors generally exhibited a high nuclear:cytoplasmic ratio, prominent nucleoli, mitotic figures, and increased angiogenesis; moreover, tumor cells could be transplanted, and then re-transplanted over two generations in Athymic Nude mice, which are all characteristics of cancer (38).

Surprisingly however, the histopathological *architecture* and *cell morphology* within randomly chosen tumors that developed in Beige Nude XID mice under varying conditions of folate nutrition (discussed below) appeared different. Thus, on low power magnification (**Figure** 2 A), a tumor which developed under entirely folate-replete conditions (i.e., HF-raft implanted in a mouse consuming a 1200-nmol folate/kg diet) exhibited a heterogeneous population of oval and spindle shaped cells which were distributed in an apparently disorganized manner. Most oval cells had a cytoplasmic margin that was indented by abutting tumor cells. There were 'narrow streams' of spindle shaped cells arranged in streaks across the field. On higher magnification (**Figure** 2 E), all cells had prominently stained nuclei and multiple nucleoli; there were many mitotic figures and scattered apoptotic bodies. Surrounding many bi-nucleated larger cells was a more prominent pink stained ground-glass appearance than the background intercellular material. By contrast, when viewed on low power magnification (**Figure** 2 C), a tumor which developed after an HF-raft was implanted in a folate-deficient mouse consuming a 400-nmol folate/kg diet exhibited a much more uniform population of oval elongated and spindle-shaped cells, many with abundant cytoplasm, that were arranged in distinct 'streams' that appeared to fan out in different directions across the field. On higher magnification (**Figure** 2 G), many of these cells had a uniform sieve-like nuclear chromatin pattern which rendered the nucleus relatively lighter staining (a hallmark of megaloblastosis (15)), and mitotic figures and apoptotic bodies were slightly more prominent. There was also generally more uniform pink ground-glass material in

between cells throughout the field. The histopathology of a tumor which developed after an HF-raft was implanted in a less folate-deficient mouse (i.e., consuming a 600-nmol folate/kg diet) (**Figure** 2 B, F) generally appeared intermediate between features of tumors found in mice fed a 1200- and 400-nmol folate/kg diet. Of added significance, when an LF-raft was implanted in a folate-replete mouse, the tumor architecture on low magnification (**Figure** 2 D) exhibited several groups of cells that had a distinctly whorled appearance, composed of groups of spindle shaped cells arranged much like many bouquets of flowers. On higher magnification (**Figure** 2 H), these cells still revealed a sieve-like nuclear chromatin pattern but with no megaloblastic changes. The cytoplasm was not abundant and there were few apoptotic bodies. The few scattered red cells between these whorled groups of cells highlighted obvious distinctions from the pink ground-glass stained intercellular material. Thus, although tumors found in folate-deficient mice can exhibit megaloblastic features (49), these light microscopy findings (**Figure** 2 A-H) now also suggested that the folate nutritional status of tissues before oncogenic induction and during tumor growth may have an important influence on the *cellular architecture* of tumors.

As shown in **Figure** 3, irrespective of the folate-content of the diet consumed, *every single* Beige Nude XID mouse that had been implanted with HF-rafts developed an aggressive tumor at the implantation site.

When HF-rafts were implanted in mice that were chronically fed either a 1200-, or 600-, or 400-nmol folate/kg diet (**Figure** 3), there were 0-, 1-, and 3- HPV16-raft-derived tumors at 4-weeks, respectively; however, because of insufficient net numbers of mice, the issue of an earlier onset of tumors in the most folate-deficient mice could not be statistically assessed. The mean onset of tumors (measured in days after raft-implantation) among mice fed the 1200-, 600-, and 400-nmol folate/kg diets were 52.6 ±22, 63.3 ±26, and 49.8 ±21 -days, respectively. However,

294 there was no statistically significant finding from the ANOVA that the tumor onset time differs
295 among the 3 diet groups (P = 0.31).

296 Whereas the majority of the tumors in the 1200-nmol folate/kg diet group (**Figure** 3 A)
297 became obvious within a relatively narrower window after implantation (between 8-12 weeks),
298 there were 2 of 14 tumors that appeared very delayed at 24th and 25th weeks after implantation.
299 By contrast, the onset of tumors in the 600- and 400-nmol folate/kg diet groups was spread out
300 between 4-16 and 4-18 weeks, respectively (**Figure** 3, B and C).

301 Thus *(i)* it was essential for these (HPV16)BC-1-Ep/SL keratinocytes to be in 3-
302 Dimensional form as differentiated HPV16-organotypic rafts (that were functional in generating
303 amplified HPV16 DNA (38)) before these keratinocytes could be transformed into an aggressive
304 cancer *in vivo* (**Figure** 3). These studies also raised the possibility that *(ii)* the folate nutritional
305 status of tissues before oncogenic induction and during tumor growth may have an important
306 influence on the onset and growth of the tumor.

307 Because of costs associated with purchase of these expensive Beige Nude XID mice, we
308 tested for serum homocysteine concentrations only at the time of sacrifice of these tumor-bearing
309 mice. The results revealed that Beige Nude XID mice fed the 1200-nmol folate/kg (folate-replete)
310 diet had a baseline level of serum homocysteine of 26.1-μM, whereas the (folate restricted) 600-
311 and 400-nmol folate/kg diets induced a serum homocysteine of 44.1-μM and 63.6-μM,
312 respectively (**Table** 1). These studies confirmed that the mice fed a progressively folate-
313 restricted diet exhibited proportionately increasing metabolic evidence of folate deficiency when
314 compared to mice fed a folate-replete diet. Parenthetically, such data were quite comparable with
315 earlier studies in female CD1 mice where after two months on these defined diets, the serum
316 homocysteine ranged from 19-μM (on the 1200-nmol folate/kg diet), 41-μM (on the 600-nmol
317 folate/kg diet) and 77-μM (on the 400-nmol folate/kg diet) (44).

The single greatest risk factor for malignant progression of tissues by HPV16 is persistence of infection when HPV16 E6 and E7 viral oncogenes become constitutive components of host keratinocytes and are deregulated together with other cellular proteins; thus, HPV16 E6 and E7 expression is considered essential for carcinogenesis (50-52). Accordingly, we investigated if HPV16 oncogenes were detected in 10 randomly chosen tumors in Beige Nude XID mice from among the three dietary groups. As shown in **Figure** 4 A and B, HPV16 E6 and E7 RNA and proteins were detected in all HPV16-tumors that developed from HF-rafts implanted in folate-replete and folate-deficient mice. This supported the possibility that these could be HPV16-derived tumors. In addition, there was no difference in either HPV16 E6 or E7 RNA [means ±SD (n = 10)] in the group of tumors that developed in mice fed either a high- *versus* low-folate diet (1200- or 400-nmol folate/kg diet, respectively). As noted in **Figure** 4 A, the lack of detection of HPV16 E6 RNA in tumor #2 (1200-nmol folate/kg diet), and tumor #8 (600-nmol folate/kg diet), as well as a lack of detection of both E6/E7 RNA in tumor #7 (600-nmol folate/kg diet), despite the identification of HPV16 E6/E7 protein expression in all tumors (discussed below), is likely related to sampling error since control cellular transcripts were also not detected; unfortunately, we did not have sufficient tumor tissue to repeat RNA analysis.

There were statistically significant findings for the differences in mean percent HPV16 E6 protein/β-actin ratios and mean percent HPV16 E7 protein/β-actin ratios in tumors among the 3 dietary groups from the ANOVA ($P < 0.001$). The post-hoc comparisons between the mean percent HPV16 E6 protein/β-actin ratio in tumors (n =10) in each of the 3 dietary groups (**Figure** 4 B), revealed no difference in HPV16 E6 expression (mean group percentages) in the group of tumors in mice fed a 1200- and 600-nmol folate/kg diet (32.75 ±6.23 and 35.91 ±8.95, respectively). However, there was significantly more HPV16 E6 protein expression (57.22

±13.89) from the group of tumors in mice fed the lowest folate diet (400-nmol folate/kg diet) when compared to mice fed either an intermediate-folate diet (600-nmol folate/kg diet) (P = 0.001), or a high-folate diet (1200-nmol folate/kg diet) (P = 0.001). Similarly, the post-hoc comparisons between the mean percent HPV16 E7 protein/β-actin ratio in tumors (n =10) in each of the three dietary groups (**Figure** 4 B), revealed no difference in HPV16 E7 protein expression in the group of tumors in mice fed a 1200- and 600-nmol folate/kg diet (18.81 ±4.05 and 19.85 ±4.63, respectively). But there was significantly more HPV16 E7 protein expression (52.93 ±9.09) from the group of tumors in mice fed a 400-nmol folate/kg diet when compared to either a 600-nmol folate/kg diet (P = 0.001), or a 1200-nmol folate/kg diet (P = 0.001).

Characterization of HPV16 DNA integration into the genome of tumors. Because *(i)* HF-rafts had a baseline HPV16 DNA integration ratio of less than 50% (**Figure** 1 A), and *(ii),* genomic integration of HPV16 DNA progressively increased as monolayers of (HPV16)BC-1-Ep/SL cells became more folate-deficient *in vitro* (**Figure** 1 B), we determined the extent to which integration of HPV16 DNA into the cellular genome of tumors was present in mice fed a low-folate *versus* high-folate diet. The sequence determination of viral-cellular junctions provides direct proof of the genomic integration of HPV16 DNA and also helps to localize the HPV16 integrated sequences in chromosomes (48). Accordingly, *each* of these tumors were subjected to a more extensive multiplex Junction-PCR analysis using the panel of 75 primers that were previously defined as loci for integration of HPV16 in genomic DNA from established human cervical cancers (48). **Supplemental Figure** 2 shows an example of PCR product analysis of a single randomly chosen tumor from mice fed either a 1200-nmol folate/kg diet (**Supplemental Figure** 2 A), or 600-nmol folate/kg diet (**Supplemental Figure** 2 B), or a 400-nmol folate/kg diet (**Supplemental Figure** 2 C). **Supplemental Figure** 2 D contains results from a representative tumor from a folate-replete mouse that was implanted with an LF-raft. In this

analysis, *each well contained one of 75 different primers,* and the positive detection of amplification of a specific viral-cellular DNA junction (within one or more of the 75 PCR products on agarose gel electrophoresis) is signaled by the finding of a second slower moving band. As shown in **Supplemental Figure** 2 A-C, there were 3-, 5-, and 8- slower moving bands among 75 different wells in each of the tumors from mice fed a 1200-, 600-, and 400-nmol folate/kg diet, respectively, with 7 slower moving bands in **Supplemental Figure** 2 D.

A more detailed analysis of results involving identification of HPV16 DNA integration sites in HF-raft-derived tumors that developed in Beige Nude XID mice fed various amounts of dietary folate is shown in **Supplemental Table** 6. These results demonstrated that *all* tumors contained HPV16 DNA that integrated into genomic DNA. Those integration sites (depicted in *red* font) identified viral-genomic DNA junctions where HPV16 insertion was directly into cellular genes, whereas integration sites (depicted in *black* font) indicated HPV16 insertion within 500 kb upstream of cellular genes, and integration sites (depicted in *blue* font) indicated an insertion site not within a known cellular gene. The average number of HPV16 integration sites into the cellular genome of tumors that developed when HF-rafts were implanted in Beige Nude XID mice fed a 1200-, 600-, and 400-nmol folate/kg diet, was 2.90 ±0.88 (n = 10), 4.83 ±0.88 (n = 12), and 5.90 ±0.99 (n = 10), respectively (**Supplemental Table** 6). There were significantly more integration sites from HF-raft-derived tumors from mice that were on a folate-deficient diet (either 400- or 600-nmol folate/kg diet) than mice on a folate-replete diet (1200-nmol folate/kg diet) ($P < 0.05$). Moreover, in tumors that formed in folate-deficient mice, the majority of integration sites targeted more than one cellular gene (**Supplemental Table** 6, *red* font) or within 500 kb upstream of cellular genes (**Supplemental Table** 6, *black* font).

Because many more insertion sites into genomic DNA were documented [in HF-raft-derived tumors that developed] following implantation in folate-deficient mice compared to

folate-replete mice (**Supplemental Table** 6), these data raised the likelihood of a dynamic process of genomic integration of HPV16 into implanted HPV16-organotypic rafts that occurred longitudinally as a function of time.

Consequences of HPV16 DNA integration into the genome of (HPV16)BC-1-Ep/SL cells on tumor growth. Next we tested the hypothesis that once increased HPV16 integration occurred in the genomic DNA of (HPV16)BC-1-Ep/SL cells during induction of folate deficiency *in vitro* (**Figure** 1 B), there would be a corresponding marked heterogeneity in onset of tumors after such (HPV16)BC-1-Ep/SL cell-derived LF-rafts were implanted into folate-replete Beige Nude XID mice (fed 1200-nmol folate/kg diet). As shown in **Supplemental Figure** 3, the pattern of tumor development and tumor growth in 24 folate-replete Beige Nude XID mice was markedly different when compared to the development of cancers in folate-replete mice implanted with HF-rafts (see **Figure** 3 A). Tumors developed in three clusters: One group manifested from 7-14 weeks, a second between 20-26 weeks, and the third between the 28-31 weeks. This heterogeneity strongly suggested a multi-centric origin of these tumors.

As shown in **Supplemental Table** 7, the average number of HPV16 integration sites into the genomic DNA of tumors when LF-rafts were implanted in folate-replete Beige Nude XID mice fed a 1200-nmol folate/kg diet was 6.11 ±0.88 (n = 19). When these data were compared to the average of 2.90 ±0.88 (n = 10) insertion sites found in tumors generated from HF-rafts implanted in folate-replete Beige Nude XID mice fed a 1200-nmol folate/kg diet (**Supplemental Table** 6), the results were statistically significant ($P < 0.05$); conversely, there was no difference when these data were compared to similar parameters found (5.90 ±0.99 (n = 10)) from tumors generated in (folate-deficient) mice fed a 400-nmol folate/kg diet (**Supplemental Table** 6). Therefore collectively, these results strongly suggest that the low-folate state was highly permissive for integration of HPV16 DNA into the cellular genome both *in vitro* and *in vivo*.

Discussion

Transformation of implanted HPV16-organotypic rafts into cancer in Beige Nude XID mice. The strong evidence *against* the possibility that (HPV16)BC-1-Ep/SL cells were a spontaneous tumorigenic cell line is discussed in detail in **Supplemental Discussion**. By contrast, the development of tumors, shortly after implantation of 3-Dimensional, differentiated, functional HF-rafts in folate-replete Beige Nude XID mice, exhibited all the characteristics of an aggressive cancer. For example, these tumors developed shortly after exposure to the carcinogen (in this case HPV16 viral DNA) within weeks, and exhibited a tumor doubling time of less than 7 days, and often between 2-5 days in folate-replete mice. By comparison, Burkitt's Lymphoma, one of the most aggressive human cancers, has a tumor doubling time of 1-2 days (53). The combination of rapid tumor growth with microscopic visualization of the histology of these tumors using hematoxylin:eosin staining—the standard approach used by clinical pathologists worldwide to rapidly distinguish a cancer from a benign tumor—demonstrated classic characteristics of malignancy (as detailed in Results). The additional dual findings of tumor biomarkers of HPV16 oncogene expression at both the RNA and protein level *and* demonstration of genomic integration by HPV16 DNA (the existing clinical gold standard) characterized these as HPV16-derived cancers.

The possibility that transformation of implanted (HPV16)BC-1-Ep/SL-derived organotypic rafts into cancer in Beige Nude XID mice can be influenced by varying the folate milieu warranted specific information on the effect of folate deficiency in altering: *a)* the frequency of development of these cancers, including their onset and growth patterns; *b)* the expression of HPV16 E6 and E7 oncogenes within these tumors; and *c)* the characteristics of genomic integration of HPV16 in tumors. Our studies have provided new information on each of

437 these parameters within [HPV16-organotypic raft-derived] tumors as they relate to folate
438 deficiency in mice.

439 Our data have also raised three new possibilities that warrant additional study. These
440 relate to *(i),* a potential direct relationship between the earliest *onset* of tumors in those mice that
441 were most folate-deficient when compared to folate-replete mice. Although we were not able to
442 establish this relationship statistically at significance level 0.05 because of small sample size
443 (**Figure** 3), the observed difference in the earliest tumor onset times in this study justifies the
444 need for a larger study to further ascertain this relationship. In addition *(ii),* there is the likelihood
445 that the nutritional state of tissues before oncogenic induction and during tumor growth can alter
446 and influence the final histopathology (*architecture*) of the tumor (**Figure** 2). And *(iii),* there is
447 the question of a potential influence of folate availability on the *rates* of tumor growth (**Figure** 3).
448 These issues require further intentional study with a larger number of mice to generate robust
449 statistically significant data. Such data will be an important first step to identifying the
450 fundamental mechanistic basis for the requirement of an intact 3-Dimensional structure of
451 differentiated, functional HPV16-organotypic rafts before transformation to aggressive cancers
452 in these mice.

453 ***Pathways to HPV16-induced oncogenesis and role of genomic integration via three different***
454 ***models.*** The nutritional status of HPV16-organotypic rafts before and after implantation in mice
455 has an influence in HPV16-oncogenic induction and tumor growth (**Figure** 3 and **Supplemental**
456 **Figure** 3). Indeed, the observed differences raise the possibility of 3 different pathways to
457 oncogenesis *within* these HPV16-organotypic rafts in folate-replete *versus* folate-deficient Beige
458 Nude XID mice.

459 ***[Model 1] Proposed pathway to cancer when HF-rafts are implanted in folate-replete***
460 ***mice*****:** If indeed implanted HF-rafts in folate-replete mice, which generate abundant HPV16

viruses (38), behave similar to implanted human foreskin's infected with HPV16 (45), these HF-rafts would likely continue to generate a large number of infectious HPV16 virus particles within a cyst under the skin over the entire period *in vivo* (38). Therefore, it is possible that these infectious HPV16 viruses could repeatedly re-infect the implanted HPV16-organotypic raft epithelium (following micro-trauma sustained during normal cage activity of mice), and thereby contribute to a higher density of HPV16-infection of the implanted raft. This could lead to greater dysregulation of HPV16 early gene expression in the more heavily infected tissues, analogous to repeated HPV16 infection of susceptible cervical tissue from either adjacent infected tissues or an infected partner. (See "Cysts, dose-dense infection, and 'field cancerization'" in **Supplemental Discussion**). Such a scenario (for repeated infection) can potentially explain how an HPV-infected cervix contains all three cervical intraepithelial neoplasia (CIN) 1-3 features in the same histological specimen (see Ref. (54), Figure 7A). This recalls the 1953 hypothesis of Slaughter's 'field cancerization' defect (55), which suggested inherent dangers in repeated exposure of susceptible tissues to a carcinogen. In this context, because HPV16 episomes alone can cause cervical cancer in one-third of cases (12, 56, 57), repeated reinfection of the implanted keratinocyte tissue can lead to a high-titer of HPV16 episomes per keratinocyte (i.e., an increased dose-density of infection), which can lead to increased oncogene stimulation *despite* relatively lower degrees of genomic integration. Therefore, under folate-replete conditions (where all previous studies have been carried out), the HPV16 oncogenes could play a critical and primary role in the development of cancer by a variety of established mechanisms (52, 54, 58-68). Whether one or more of these HPV16 oncogenes are more dominant in contributing to the observed narrower window of onset of tumors warrants longitudinal examination of HPV16-organotypic rafts *in situ* over time after implantation in mice *well before the development of tumors*.

Parenthetically, despite the detection of HPV16 E6/E7 RNA and protein expressed in every single tumor, we have not yet proven that these oncogenes were the *sole* cause for induction of cancers. This is because there are additional mechanisms whereby HPV16 exerts its effects (58, 59), particularly those arising from genomic integration of HPV16 DNA and subsequent insertional mutagenesis with inactivation of tumor suppressor genes and/or activation of oncogenes. This caveat is relevant to this context because the genomic integration ratio in HF-rafts was approximately 40% at baseline prior to these *in vivo* experiments (**Figure** 1)].

***[Model 2] Proposed pathway to cancer when HF-rafts are implanted in folate-deficient mice*:** When HF-rafts are implanted in folate-deficient mice, there is potential for much more genomic integration of HPV16 DNA because folate deficiency also predisposes to single- and double-stranded fragmentation of DNA in rare *and* common fragile sites (24-33, 69-72) [discussed in Ref. (38)]; and as with patients with DNA repair defects like Fanconi Anemia (73-76) this is a highly permissive state for HPV16 DNA integration into multiple sites within genomic DNA. These findings were unequivocally confirmed in **Supplemental Table** 6. Such integration events can disrupt one among many known tumor suppressor genes (29-31, 48, 77). However, early integration of HPV16 DNA into the cellular genome also disrupts the open reading frame of HPV16 E2 gene [which controls expression of E6 and E7]; so with loss of E2, there is de-repression and higher expression of E6 and E7 genes (34, 35). This can explain the significantly higher HPV16 E6 and E7 proteins in tumors of folate-deficient mice (**Figure** 4 B).

Moreover, during the prolonged folate-deficient state in these mice (37), homocysteinylation of extant cellular hnRNP-E1 within the HPV16-organotypic raft would likely trigger its own auto up-regulation (49); so newly synthesized hnRNP-E1 would also be homocysteinylated. This would profoundly reduce HPV16 L1 and L2 viral capsid proteins, and inhibit generation of fully encapsidated infectious HPV16 virions (38); however, there would

still be accumulation of capsid-less HPV16 DNA as episomes within HPV16-organotypic raft keratinocytes (38). These HPV16 episomes could either continue to express HPV16 oncogenes (12, 56, 57) and stimulate carcinogenesis (58, 59), or alternatively integrate into [fragile sites of] the cellular genome from where HPV16-oncogenes could also be expressed and/or cellular tumor suppressor genes could be inactivated leading to cancer even under these conditions.

***[Model 3] Proposed pathway to cancer when LF-rafts are implanted in folate-replete mice*:** In the model involving implantation of LF-rafts in folate-replete Beige Nude XID mice (**Supplemental Figure** 3), there was a high level of genomic integration of HPV16 (integration ratio of 90%) in LF-rafts at baseline (i.e., even before (HPV16)BC-1-Ep/SL cells were differentiated into LF-rafts (**Figure** 1 B). Therefore, there was a high likelihood of increased heterogeneity in development of cancers after LF-rafts were implanted in folate replete Beige Nude XID mice on the following basis: Although insertional mutagenesis by HPV16 DNA into the promoters of tumor suppressor genes can result in inactivation of tumor suppressor genes and trigger [early] tumor formation, by the same token, HPV16 integration could equally well result in the inactivation of *cell cycle* genes or *growth promoting genes;* this could result in a variable delay in onset of tumors. Indeed, the formation of both early and later tumors was borne out in data leading to **Supplemental Figure** 3. Because LF-rafts contained equally high levels of HPV16 episomal DNA as HF-rafts (38), these HPV16 episomes would accumulate within the differentiated upper keratinocyte layers of LF-rafts. So when these LF-rafts are implanted in folate-replete mice, the prevailing murine serum folate of 250-nM (78) (this is ten-fold more than humans (79)) would rapidly relieve folate deficiency in the raft, with homocysteine levels approaching normal values in 1 week (15, 36). In addition, because the t½ of hnRNP-E1 is approximately 52 hours (37), endogenous homocysteinylated-hnRNP-E1 would be largely degraded by end of week-1 (37, 49). And as a result, the differentiated keratinocytes within the

HPV16-organotypic raft implant could then begin to generate significant HPV16 viral capsid proteins and encapsidate the extant amplified HPV16 DNA (38) over the ensuring weeks. The predictable net result would be an abundance of complete HPV16 viral particles within the implant [with no place to go] in an immunosuppressed mouse with no capacity to clear this accumulation of HPV16 virions. Therefore, when a clone of cells within the raft is transformed into a malignancy, there would be a significant number of HPV16 viral particles that contaminated the primary and secondary tumors, as we observed (see Ref. (38), Fig. 7G)—*[in analogy to the scenario in Proposed Model 1, above]*. However, relief of folate deficiency would not alter the extant high-level HPV16 DNA integrated into genomic DNA (**Supplemental Table** 7) which could independently trigger oncogenesis through insertional mutagenesis—*[in analogy to the scenario in Proposed Model 2, above]* (34, 35). So, carcinogenesis in *[Proposed Model 3]* could be initiated by both excess accumulated infectious HPV16 virions and by increased genomic integration of HPV16 DNA.

Future studies are needed to test the veracity of these three proposed model pathways and also document more precisely if there is a progressively greater insertion of HPV16 directly into, or in the vicinity of, specific cellular genes of these HPV16-organotypic rafts *as a function of time prior* to the development of tumors. This will help to clarify the basis for potential differences in the etiology of the tumors formed in folate-deficient *versus* folate-replete mice, and whether such tumors primarily arise from disruption of cellular tumor suppressor genes, or activation of HPV16/cellular oncogenes, or both, in the three proposed models.

Whether the 3 distinct clusters of tumors observed in *Model 3* (**Supplemental Figure** 3) are consistent with integration at specific loci within genomic DNA will require whole genome sequencing of each of these tumors using many more mice in order to generate robust data. Such studies can define any possible concordance of tumor growth with actual genes that are disrupted.

Clinical issues related to genomic integration of HPV16 and folate status. (See "Significance of global folate and vitamin-B_{12} nutrition, the HPV16-life cycle, and HPV16-induced cancer" in **Supplemental Discussion**). Although genomic integration of HPV16 can take place early in the natural history of HPV-induced cancer (80, 81), and approximately 70% of HPV16-cervical cancers also contain integrated HPV16 sequences (9), key data linking folate nutrition to these women are lacking. For example, there has not been any simultaneous systematic evaluation of the folate status in women with these cancers; nor is there other data on the induction of genomic integration of HPV16 DNA during clinical folate deficiency *in vivo;* nor has the mechanistic basis for such observations (early HPV16 genomic integration) been explained. Our studies raise the potentially ominous possibility that if women have either transient or chronic folate- and/or vitamin-B_{12}- deficiency during the course of HPV16 infection, the combined effects of inhibition of HPV16 viral capsid proteins—(leading to accumulation of 'capsid-less' HPV16 virions and genomic instability induced by folate- and/or vitamin-B_{12}- deficiency *per se*)—could facilitate genomic integration of HPV16 DNA early in the natural history of HPV16 infection, thereby predisposing to persistence of HPV16-infection and predisposition to cancer. (See "Significance of this animal model to study the HPV16 life cycle and cancer" in **Supplemental Discussion**). Our mouse model will help expedite understanding of the impact of progressive genomic integration of HPV16 on carcinogenesis, the distinct pathways to HPV16-induced cancers in folate-replete *versus* folate-deficient mice, and allow preclinical simulation of HPV16-induced cancer risk in immunosuppressed HPV16- and HIV-infected individuals with food insecurity-induced folate deficiency. Indeed, improved understanding of the role of such nutritional co-factors that can facilitate HPV16-induced carcinogenesis is an important step in the field of preventive oncology.

Acknowledgements

We are indebted to Professor Elliot J. Androphy (Indiana University) for helpful suggestions and encouragement during these studies, and for critically reading the manuscript. We thank Dr. Michael J. Morton (Roudebush Veterans Affairs Medical Center) for assistance with photography of histopathology slides. This work was supported by a Merit Review Award #I01BX002027 (to ACA) from the United States Department of Veterans Affairs Biomedical Laboratory Research and Development Service.

Disclaimer. The contents of this paper do not represent the views of the U.S. Department of Veterans Affairs or the United States Government.

Authors' contributions to the manuscript

SX conducted research (hands-on conduct of the experiments and data collection), generated figures, and analyzed data; YST conducted research, generated figures, and analyzed data. PK conducted research, generated figures, and analyzed data; SPS measured thiols in murine serum; YZ performed statistical analysis; ACA designed research (project conception, development of overall research plan, and study oversight), analyzed data, wrote the paper, and is primarily responsible for the final content of the paper. All authors approved the final manuscript.

References

1. CDC. The link between HPV and cancer: http://www.cdc.gov/hpv/parents/cancer.html. Accessed February 11, 2016.
2. Schiffman M, Castle PE, Jeronimo J, Rodriguez AC, and Wacholder S. Human papillomavirus and cervical cancer. *Lancet.* 2007;370:890-7.
3. Schwarz E, Freese UK, Gissmann L, Mayer W, Roggenbuck B, Stremlau A, and zur Hausen H. Structure and transcription of human papillomavirus sequences in cervical carcinoma cells. *Nature.* 1985;314:111-4.
4. Wagatsuma M, Hashimoto K, and Matsukura T. Analysis of integrated human papillomavirus type 16 DNA in cervical cancers: amplification of viral sequences together with cellular flanking sequences. *J Virol.* 1990;64:813-21.
5. Bechtold V, Beard P, and Raj K. Human papillomavirus type 16 E2 protein has no effect on transcription from episomal viral DNA. *J Virol.* 2003;77:2021-8.
6. Romanczuk H, and Howley PM. Disruption of either the E1 or the E2 regulatory gene of human papillomavirus type 16 increases viral immortalization capacity. *Proc Natl Acad Sci U S A.* 1992;89:3159-63.
7. Kalantari M, Karlsen F, Kristensen G, Holm R, Hagmar B, and Johansson B. Disruption of the E1 and E2 reading frames of HPV 16 in cervical carcinoma is associated with poor prognosis. *Int J Gynecol Pathol.* 1998;17:146-53.
8. Vernon SD, Unger ER, Miller DL, Lee DR, and Reeves WC. Association of human papillomavirus type 16 integration in the E2 gene with poor disease-free survival from cervical cancer. *Int J Cancer.* 1997;74:50-6.
9. Badaracco G, Venuti A, Sedati A, and Marcante ML. HPV16 and HPV18 in genital tumors: Significantly different levels of viral integration and correlation to tumor invasiveness. *J Med Virol.* 2002;67:574-82.

10. Hopman AH, Smedts F, Dignef W, Ummelen M, Sonke G, Mravunac M, Vooijs GP, Speel EJ, and Ramaekers FC. Transition of high-grade cervical intraepithelial neoplasia to micro-invasive carcinoma is characterized by integration of HPV 16/18 and numerical chromosome abnormalities. *J Pathol.* 2004;202:23-33.

11. Klaes R, Woerner SM, Ridder R, Wentzensen N, Duerst M, Schneider A, Lotz B, Melsheimer P, and von Knebel Doeberitz M. Detection of high-risk cervical intraepithelial neoplasia and cervical cancer by amplification of transcripts derived from integrated papillomavirus oncogenes. *Cancer Res.* 1999;59:6132-6.

12. Pett M, and Coleman N. Integration of high-risk human papillomavirus: a key event in cervical carcinogenesis? *J Pathol.* 2007;212:356-67.

13. Gray E, Pett MR, Ward D, Winder DM, Stanley MA, Roberts I, Scarpini CG, and Coleman N. In vitro progression of human papillomavirus 16 episome-associated cervical neoplasia displays fundamental similarities to integrant-associated carcinogenesis. *Cancer Res.* 2010;70:4081-91.

14. Leiding JW, and Holland SM. Warts and all: human papillomavirus in primary immunodeficiencies. *J Allergy Clin Immunol.* 2012;130:1030-48.

15. Antony AC. Megaloblastic Anemias. Chapter 39. In: Hoffman R, Benz EJ (Jr), Silberstein LE, Heslop HE, Weitz JI, Anastasi J, Salama ME, Abutalib SA (eds). *Hematology: Basic Principles and Practice, Seventh Edition*. Philadelphia: Elsevier Saunders; 2017:514-45.

16. Antony AC. Vegetarianism and vitamin B-12 (cobalamin) deficiency. *Am J Clin Nutr.* 2003;78:3-6.

17. Antony AC. Megaloblastic Anemias. Chapter 164. In: Goldman L, and Schafer AI eds. *Goldman-Cecil Medicine, 25th Edition*. New York: Elsevier Saunders; 2015:1104-14.

18. Butterworth CE, Jr., Hatch KD, Gore H, Mueller H, and Krumdieck CL. Improvement in cervical dysplasia associated with folic acid therapy in users of oral contraceptives. *Am J Clin Nutr.* 1982;35:73-82.

19. Butterworth CE, Jr., Hatch KD, Macaluso M, Cole P, Sauberlich HE, Soong SJ, Borst M, and Baker VV. Folate deficiency and cervical dysplasia. *JAMA.* 1992;267:528-33.

20. Weinstein SJ, Ziegler RG, Selhub J, Fears TR, Strickler HD, Brinton LA, Hamman RF, Levine RS, Mallin K, and Stolley PD. Elevated serum homocysteine levels and increased risk of invasive cervical cancer in US women. *Cancer Causes Control.* 2001;12:317-24.

21. Kwanbunjan K, Saengkar P, Cheeramakara C, Thanomsak W, Benjachai W, Laisupasin P, Buchachart K, Songmuaeng K, and Boontaveeyuwat N. Low folate status as a risk factor for cervical dysplasia in Thai women. *Nutr Res.* 2005;641-54.

22. Piyathilake CJ, Badiga S, Paul P, Vijayaraghavan K, Vedantham H, Sudula M, Sowjanya P, Ramakrishna G, Shah KV, Partridge EE, et al. Indian women with higher serum concentrations of folate and vitamin B12 are significantly less likely to be infected with carcinogenic or high-risk (HR) types of human papillomaviruses (HPVs). *Int J Womens Health.* 2010;7-12.

23. Piyathilake CJ, Henao OL, Macaluso M, Cornwell PE, Meleth S, Heimburger DC, and Partridge EE. Folate is associated with the natural history of high-risk human papillomaviruses. *Cancer Res.* 2004;64:8788-93.

24. Wickramasinghe SN, and Fida S. Bone marrow cells from vitamin B12- and folate-deficient patients misincorporate uracil into DNA. *Blood.* 1994;83:1656-61.

25. Reidy JA. Role of deoxyuridine incorporation and DNA repair in the expression of human chromosomal fragile sites. *Mutat Res.* 1988;200:215-20.

26. Duthie SJ, and Hawdon A. DNA instability (strand breakage, uracil misincorporation, and defective repair) is increased by folic acid depletion in human lymphocytes in vitro. *FASEB J.* 1998;12:1491-7.

27. Blount BC, Mack MM, Wehr CM, MacGregor JT, Hiatt RA, Wang G, Wickramasinghe SN, Everson RB, and Ames BN. Folate deficiency causes uracil misincorporation into human DNA and chromosome breakage: implications for cancer and neuronal damage. *Proc Natl Acad Sci U S A.* 1997;94:3290-5.

28. Dianov GL, Timchenko TV, Sinitsina OI, Kuzminov AV, Medvedev OA, and Salganik RI. Repair of uracil residues closely spaced on the opposite strands of plasmid DNA results in double-strand break and deletion formation. *Mol Gen Genet.* 1991;225:448-52.

29. Wilke CM, Hall BK, Hoge A, Paradee W, Smith DI, and Glover TW. FRA3B extends over a broad region and contains a spontaneous HPV16 integration site: direct evidence for the coincidence of viral integration sites and fragile sites. *Hum Mol Genet.* 1996;5:187-95.

30. Thorland EC, Myers SL, Persing DH, Sarkar G, McGovern RM, Gostout BS, and Smith DI. Human papillomavirus type 16 integrations in cervical tumors frequently occur in common fragile sites. *Cancer Res.* 2000;60:5916-21.

31. Thorland EC, Myers SL, Gostout BS, and Smith DI. Common fragile sites are preferential targets for HPV16 integrations in cervical tumors. *Oncogene.* 2003;22:1225-37.

32. Woodman CB, Collins SI, and Young LS. The natural history of cervical HPV infection: unresolved issues. *Nat Rev Cancer.* 2007;7:11-22.

33. Sutherland GR, and Richards RI. The molecular basis of fragile sites in human chromosomes. *Curr Opin Genet Dev.* 1995;5:323-7.

34. Durst M, Kleinheinz A, Hotz M, and Gissmann L. The physical state of human papillomavirus type 16 DNA in benign and malignant genital tumours. *J Gen Virol.* 1985;66:1515-22.

35. Jeon S, and Lambert PF. Integration of human papillomavirus type 16 DNA into the human genome leads to increased stability of E6 and E7 mRNAs: implications for cervical carcinogenesis. *Proc Natl Acad Sci USA.* 1995;92:1654-8.

36. Antony AC, Tang YS, Khan RA, Biju MP, Xiao X, Li QJ, Sun XL, Jayaram HN, and Stabler SP. Translational upregulation of folate receptors is mediated by homocysteine via RNA-heterogeneous nuclear ribonucleoprotein E1 interactions. *J Clin Invest.* 2004;113:285-301.

37. Tang YS, Khan RA, Zhang Y, Xiao S, Wang M, Hansen DK, Jayaram HN, and Antony AC. Incrimination of heterogeneous nuclear ribonucleoprotein E1 (hnRNP-E1) as a candidate sensor of physiological folate deficiency. *J Biol Chem.* 2011;286:39100-15.

38. Xiao S, Tang YS, Khan RA, Zhang Y, Kusumanchi P, Stabler SP, Jayaram HN, and Antony AC. Influence of physiologic folate deficiency on human papillomavirus type 16 (HPV16)-harboring human keratinocytes in vitro and in vivo. *J Biol Chem.* 2012;287:12559-77.

39. Flores ER, Allen-Hoffmann BL, Lee D, Sattler CA, and Lambert PF. Establishment of the human papillomavirus type 16 (HPV-16) life cycle in an immortalized human foreskin keratinocyte cell line. *Virology.* 1999;262:344-54.

40. Herfs M, Yamamoto Y, Laury A, Wang X, Nucci MR, McLaughlin-Drubin ME, Munger K, Feldman S, McKeon FD, Xian W, et al. A discrete population of squamocolumnar junction cells implicated in the pathogenesis of cervical cancer. *Proc Natl Acad Sci U S A.* 2012;109:10516-21.

41. Xie X, Piao L, Bullock BN, Smith A, Su T, Zhang M, Teknos TN, Arora PS, and Pan Q. Targeting HPV16 E6-p300 interaction reactivates p53 and inhibits the tumorigenicity of HPV-positive head and neck squamous cell carcinoma. *Oncogene.* 2014;33:1037-46.

42. Clawson GA, Bui V, Xin P, Wang N, and Pan W. Intracellular localization of the tumor suppressor HtrA1/Prss11 and its association with HPV16 E6 and E7 proteins. *J Cell Biochem.* 2008;105:81-8.

43. Munagala R, Kausar H, Munjal C, and Gupta RC. Withaferin A induces p53-dependent apoptosis by repression of HPV oncogenes and upregulation of tumor suppressor proteins in human cervical cancer cells. *Carcinogenesis.* 2011;32:1697-705.

44. Xiao S, Hansen DK, Horsley ET, Tang YS, Khan RA, Stabler SP, Jayaram HN, and Antony AC. Maternal folate deficiency results in selective upregulation of folate receptors and heterogeneous nuclear ribonucleoprotein-E1 associated with multiple subtle aberrations in fetal tissues. *Birth Defects Res A Clin Mol Teratol.* 2005;73:6-28.

45. Brandsma JL, Brownstein DG, Xiao W, and Longley BJ. Papilloma formation in human foreskin xenografts after inoculation of human papillomavirus type 16 DNA. *J Virol.* 1995;69:2716-21.

46. Bonnez W. The HPV xenograft severe combined immunodeficiency mouse model. *Methods Mol Med.* 2005;203-16.

47. Feldman JP, Goldwasser R, Mark S, Schwartz J, and Orion I. A mathematical model for tumor volume evaluation using two-dimensions *J Applied Quant Methods.* 2009;4:455-62.

48. Xu B, Chotewutmontri S, Wolf S, Klos U, Schmitz M, Durst M, and Schwarz E. Multiplex Identification of Human Papillomavirus 16 DNA Integration Sites in Cervical Carcinomas. *PLoS One.* 2013;8:e66693.

49. Tang YS, Khan RA, Xiao S, Hansen DK, Stabler SP, Kusumanchi P, Jayaram HN, and Antony AC. Evidence favoring a positive feedback loop for physiologic auto

upregulation of hnRNP-E1 during prolonged folate deficiency in human placental cells. *J Nutr.* 2017;147:482-98.

50. Bodily J, and Laimins LA. Persistence of human papillomavirus infection: keys to malignant progression. *Trends Microbiol.* 2011;19:33-9.

51. Snijders PJ, Steenbergen RD, Heideman DA, and Meijer CJ. HPV-mediated cervical carcinogenesis: concepts and clinical implications. *J Pathol.* 2006;208:152-64.

52. Moody CA, and Laimins LA. Human papillomavirus oncoproteins: pathways to transformation. *Nat Rev Cancer.* 2010;10:550-60.

53. Ferry JA. Burkitt's lymphoma: clinicopathologic features and differential diagnosis. *Oncologist.* 2006;11:375-83.

54. Doorbar J, Quint W, Banks L, Bravo IG, Stoler M, Broker TR, and Stanley MA. The biology and life-cycle of human papillomaviruses. *Vaccine.* 2012;30:F55-70.

55. Slaughter DP, Southwick HW, and Smejkal W. Field cancerization in oral stratified squamous epithelium; clinical implications of multicentric origin. *Cancer.* 1953;6:963-8.

56. Matsukura T, Koi S, and Sugase M. Both episomal and integrated forms of human papillomavirus type 16 are involved in invasive cervical cancers. *Virology.* 1989;172:63-72.

57. Vinokurova S, Wentzensen N, Kraus I, Klaes R, Driesch C, Melsheimer P, Kisseljov F, Durst M, Schneider A, and von Knebel Doeberitz M. Type-dependent integration frequency of human papillomavirus genomes in cervical lesions. *Cancer Res.* 2008;68:307-13.

58. zur Hausen H. Papillomaviruses and cancer: from basic studies to clinical application. *Nat Rev Cancer.* 2002;2:342-50.

59. zur Hausen H. Papillomaviruses in the causation of human cancers - a brief historical account. *Virology.* 2009;384:260-5.

60. Munger K, and Howley PM. Human papillomavirus immortalization and transformation functions. *Virus Res.* 2002;89:213-28.

61. Duensing S, Duensing A, Lee DC, Edwards KM, Piboonniyom SO, Manuel E, Skaltsounis L, Meijer L, and Munger K. Cyclin-dependent kinase inhibitor indirubin-3'-oxime selectively inhibits human papillomavirus type 16 E7-induced numerical centrosome anomalies. *Oncogene.* 2004;23:8206-15.

62. Duensing S, and Munger K. Mechanisms of genomic instability in human cancer: insights from studies with human papillomavirus oncoproteins. *Int J Cancer.* 2004;109:157-62.

63. Androphy EJ, Hubbert NL, Schiller JT, and Lowy DR. Identification of the HPV-16 E6 protein from transformed mouse cells and human cervical carcinoma cell lines. *EMBO J.* 1987;6:989-92.

64. Mansur CP, Marcus B, Dalal S, and Androphy EJ. The domain of p53 required for binding HPV 16 E6 is separable from the degradation domain. *Oncogene.* 1995;10:457-65.

65. Veldman T, Horikawa I, Barrett JC, and Schlegel R. Transcriptional activation of the telomerase hTERT gene by human papillomavirus type 16 E6 oncoprotein. *J Virol.* 2001;75:4467-72.

66. Venuti A, Paolini F, Nasir L, Corteggio A, Roperto S, Campo MS, and Borzacchiello G. Papillomavirus E5: the smallest oncoprotein with many functions. *Mol Cancer.* 2011;10:140.

67. Chow LT, Broker TR, and Steinberg BM. The natural history of human papillomavirus infections of the mucosal epithelia. *APMIS.* 2010;118:422-49.

68. Doorbar J. The papillomavirus life cycle. *J Clin Virol.* 2005;32:S7-15.

69. Das KC, and Herbert V. In vitro DNA synthesis by megaloblastic bone marrow: effect of folates and cobalamins on thymidine incorporation and de novo thymidylate synthesis. *Am J Hematol.* 1989;31:11-20.

70. Koury MJ, Horne DW, Brown ZA, Pietenpol JA, Blount BC, Ames BN, Hard R, and Koury ST. Apoptosis of late-stage erythroblasts in megaloblastic anemia: association with DNA damage and macrocyte production. *Blood.* 1997;89:4617-23.

71. Ciappio E, and Mason JB. Folate and Carcinogenesis: Basic Mechanisms**.** In: Bailey LB ed. *Folate in Health and Disease, Second Edition*. Boca Raton, FL: CRC Press; 2010:235-62.

72. Ames BN, and Wakimoto P. Are vitamin and mineral deficiencies a major cancer risk? *Nat Rev Cancer.* 2002;2:694-704.

73. Sauter SL, Wells SI, Zhang X, Hoskins EE, Davies SM, Myers KC, Mueller R, Panicker G, Unger ER, Sivaprasad U, et al. Oral human papillomavirus is common in individuals with Fanconi anemia. *Cancer Epidemiol Biomarkers Prev.* 2015;24:864-72.

74. Katzenellenbogen RA, Carter JJ, Stern JE, Butsch Kovacic MS, Mehta PA, Sauter SL, Galloway DA, and Winer RL. Skin and mucosal human papillomavirus seroprevalence in persons with Fanconi Anemia. *Clin Vaccine Immunol.* 2015;22:413-20.

75. Spriggs CC, and Laimins LA. FANCD2 binds Human Papillomavirus genomes and associates with a distinct set of DNA repair proteins to regulate viral replication. *MBio.* 2017; 8:e02340-16.

76. Langsfeld E, and Laimins LA. Human papillomaviruses: research priorities for the next decade. *Trends Cancer.* 2016;2:234-40.

77. Schmitz M, Driesch C, Jansen L, Runnebaum IB, and Durst M. Non-random integration of the HPV genome in cervical cancer. *PLoS One.* 2012;7:e39632.

78. Leamon CP, Reddy JA, Dorton R, Bloomfield A, Emsweller K, Parker N, and Westrick E. Impact of high and low folate diets on tissue folate receptor levels and antitumor responses toward folate-drug conjugates. *J Pharmacol Exp Ther.* 2008;327:918-25.

79. Antony AC. Evidence for potential underestimation of clinical folate deficiency in resource-limited countries using blood tests. *Nutrition Reviews.* 2017;75:600-15.

80. Peitsaro P, Johansson B, and Syrjanen S. Integrated human papillomavirus type 16 is frequently found in cervical cancer precursors as demonstrated by a novel quantitative real-time PCR technique. *J Clin Microbiol.* 2002;40:886-91.

81. Kulmala SM, Syrjanen SM, Gyllensten UB, Shabalova IP, Petrovichev N, Tosi P, Syrjanen KJ, and Johansson BC. Early integration of high copy HPV16 detectable in women with normal and low grade cervical cytology and histology. *J Clin Pathol.* 2006;59:513-7.

TABLE 1 Concentration of serum homocysteine in Beige Nude XID mice fed various diets for 2 months prior to HPV16 raft implantation and until their sacrifice several weeks later (between 8 and 16 weeks after raft-implantation).[1]

Diet Group	*n*	L-Homocysteine (μM)
1200-nmol of folate/kg diet	10	26.1 ±9.4 [a]
600-nmol of folate/kg diet	6	44.1 ±17.2 [b]
400-nmol of folate/kg diet	5	63.6 ±13.5 [c]

[1]The results are presented as means ± SDs, *n* = sample number as indicated. Labeled means without a common superscript letter differ, $P < 0.05$.

FIGURE LEGENDS

FIGURE 1 Determination of the time when genomic integration of HPV16 DNA occurred *in vitro.*

(*Panel* A). Assessment of the integration ratio in LF-rafts that were placed back into high-folate medium at various times indicated during the 18-days of HPV16-organotypic raft development.

(*Panel* B). Time course of progressive integration of HPV16 DNA into the cellular genome after (HPV16)BC-1-Ep/SL-*HF* cells were abruptly passaged into low-folate (F-LF) media. Samples were collected during various indicated times to detect the HPV16 E2 and E6 DNA by qPCR and thereby determine the integration ratio (38).

Values are means ± SDs, $n = 3$ (means of triplicates). Labeled means without a common letter differ, $P < 0.05$

FIGURE 2 Photomicrographs of histopathological sections of tumors stained with hematoxylin-eosin which developed after HF-rafts were implanted in Beige Nude XID Mice fed either 1200- (*Panels* A, E), 600- (*Panels* B, F) or 400- (*Panels* C, G) -nmol folate/kg diet, respectively, for 2 months prior to raft-implantation and until their sacrifice several weeks later (between 8-16 weeks). In *panels* D and H, the tumor developed after an LF-raft was implanted in a mouse fed 1200-nmol folate/kg diet.

(Magnification was 20X for A - D, and 40X for E - H).

FIGURE 3 Development of aggressive tumors within only a few weeks after 18-day old HF-rafts were implanted subcutaneously in Beige Nude XID mice that were chronically fed either 1200-nmol folate/kg diet (*Panel* A), or 600-nmol folate/kg diet (*Panel* B), or 400-nmol folate/kg diet (*Panel* C) for 2 months prior to raft-implantation and until their sacrifice several weeks later (as indicated by the tumor number). These HF-raft implantation studies were carried out in two

batches: *Panel* A, Batch 1 included tumors #1-7, and Batch 2 included tumors #8-14; *Panel* B, Batch 1 included tumors #1-5, and Batch 2 included tumors #6-12; *Panel* C, Batch 1 included tumors #1-8, and Batch 2 included tumors #9-13. For each of these panels, a tumor number was assigned in sequence when the mouse was sacrificed.

FIGURE 4 Expression of HPV16 E6 and E7 RNA (*Panel* A) and HPV16-derived E6 and E7 proteins (*Panel* B) from HPV16-organotypic raft-derived tumors that developed in Beige Nude XID mice that were chronically fed either a 1200-nmol folate/kg diet, or 600-nmol folate/kg diet, or a 400-nmol folate/kg diet for 2 months prior to raft-implantation and until their sacrifice several weeks later (between 8-16 weeks). Densitometric scanned signals of the HPV16 E6/E7 protein expression from each tumor (n = 10) normalized to the amount of β-actin protein loaded onto each gel (expressed as percent of HPV16 E6/E7 protein/β-actin ratio) is shown for each of the three dietary groups. The mean group percentages of the HPV16 E6-protein/β-actin ratio in tumors of mice fed the 400-nmol folate/kg diet (57.22 ±13.89) were significantly greater (P = 0.001) than those of mice fed either 600-nmol/kg diet (35.91 ±8.95) or 1200-nmol/kg diet (32.75 ±6.23). Likewise, the mean group percentages of the HPV16 E7-protein/β-actin ratio in tumors of mice fed the 400-nmol folate/kg diet (52.93 ±9.09) were significantly greater (P = 0.001) than those of mice fed either 600-nmol/kg diet (19.85 ±4.63) or 1200-nmol/kg diet (18.81 ±4.05).

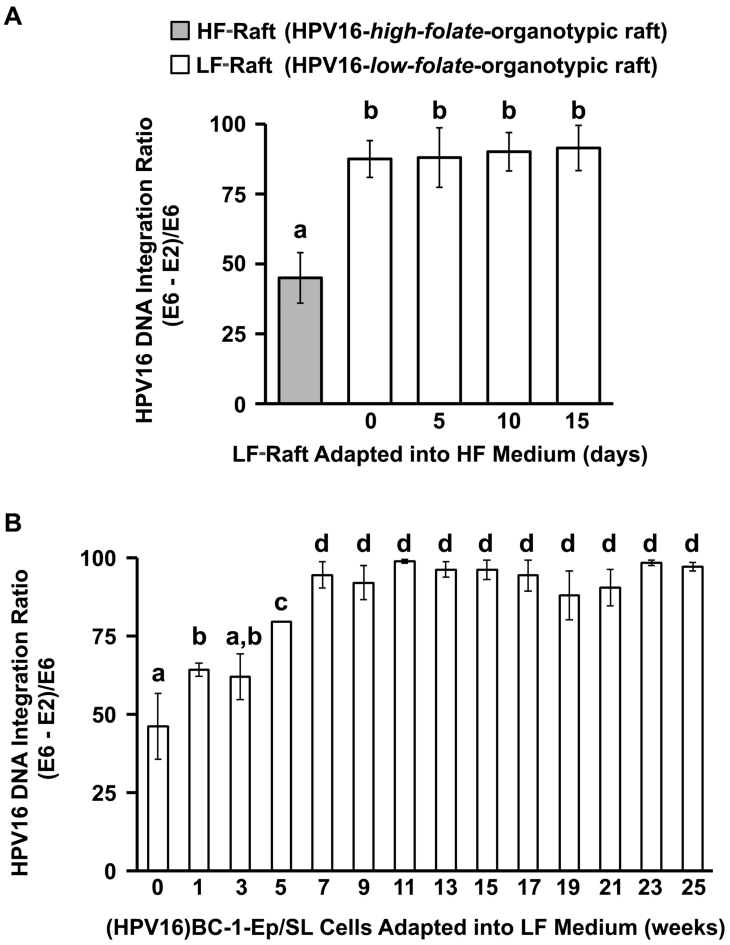
A
HF-Raft (HPV16-high-folate-organotypic raft)
LF-Raft (HPV16-low-folate-organotypic raft)
HPV16 DNA Integration Ratio
(E6 - E2)/E6
100
75
50
25
0
a
b
b
b
b
0
5
10
15
LF-Raft Adapted into HF Medium (days)
B
HPV16 DNA Integration Ratio
(E6 - E2)/E6
100
75
50
25
0
a
b
a,b
c
d
d
d
d
d
d
d
d
d
d
0
1
3
5
7
9
11
13
15
17
19
21
23
25
(HPV16)BC-1-Ep/SL Cells Adapted into LF Medium (weeks)

Figure 1

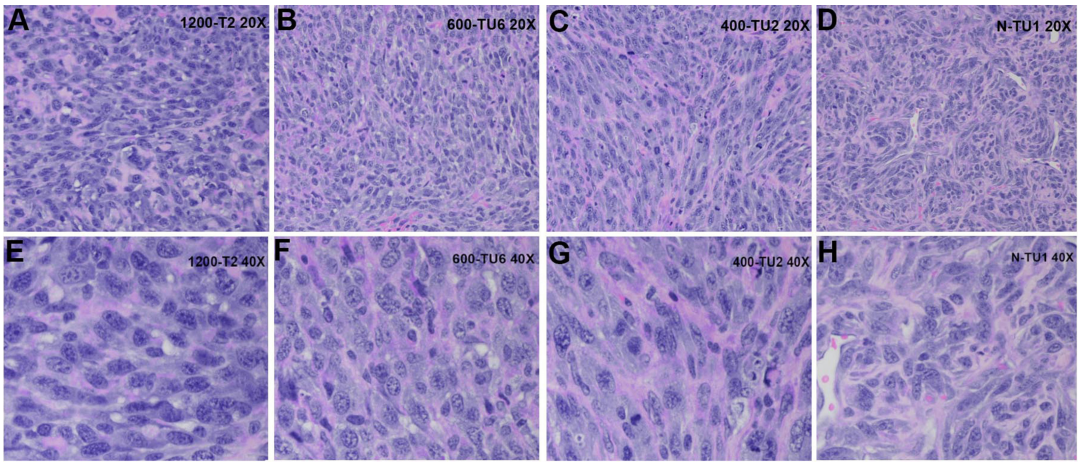
A
1200-T2 20X
B
600-TU6 20X
C
400-TU2 20X
D
N-TU1 20X
E
1200-T2 40X
F
600-TU6 40X
G
400-TU2 40X
H
N-TU1 40X

Figure 2

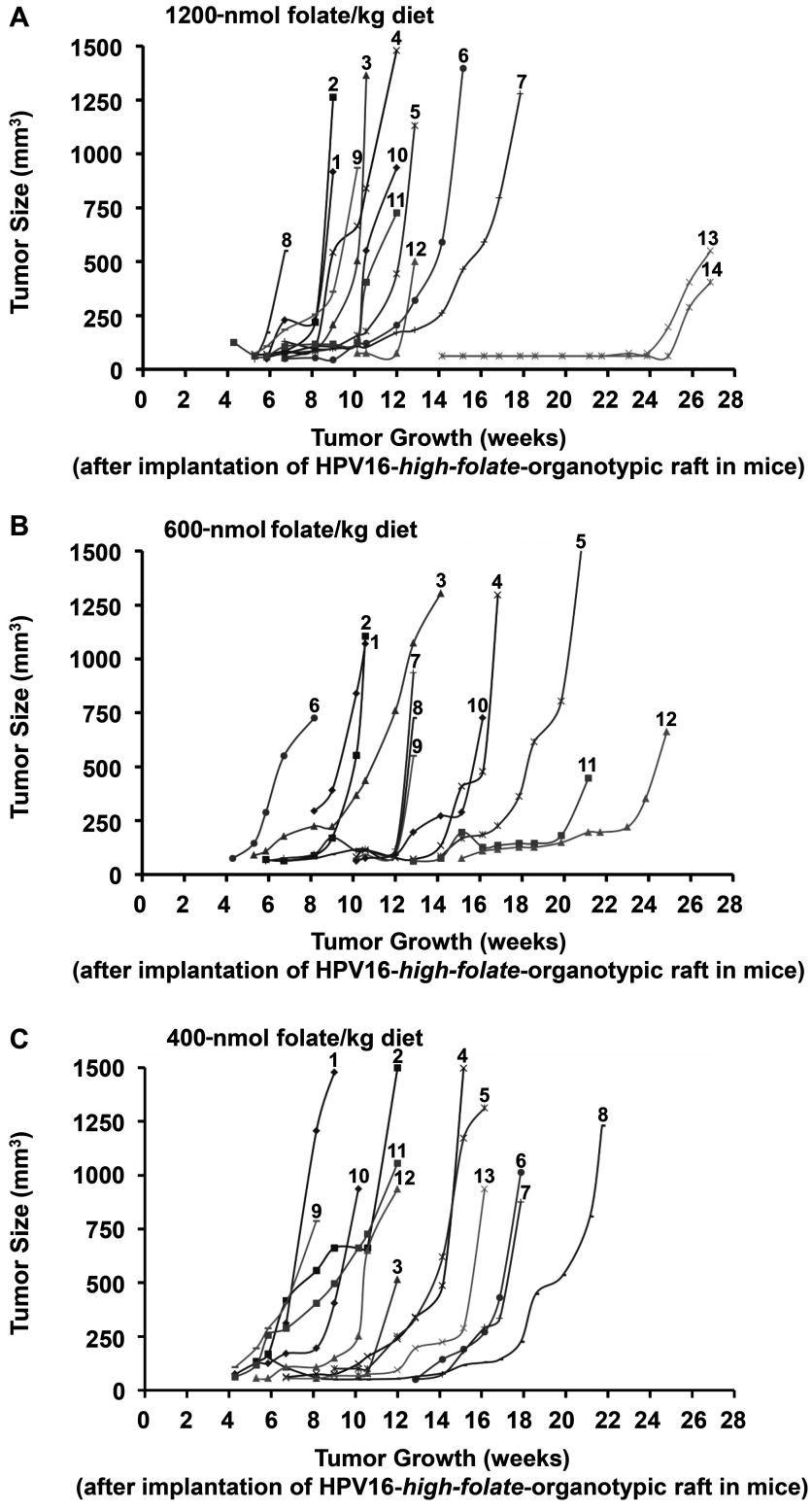
A
1200-nmol folate/kg diet
Tumor Size (mm3)
Tumor Growth (weeks)
(after implantation of HPV16-high-folate-organotypic raft in mice)
B
600-nmol folate/kg diet
Tumor Size (mm3)
Tumor Growth (weeks)
(after implantation of HPV16-high-folate-organotypic raft in mice)
C
400-nmol folate/kg diet
Tumor Size (mm3)
Tumor Growth (weeks)
(after implantation of HPV16-high-folate-organotypic raft in mice)

Figure 3

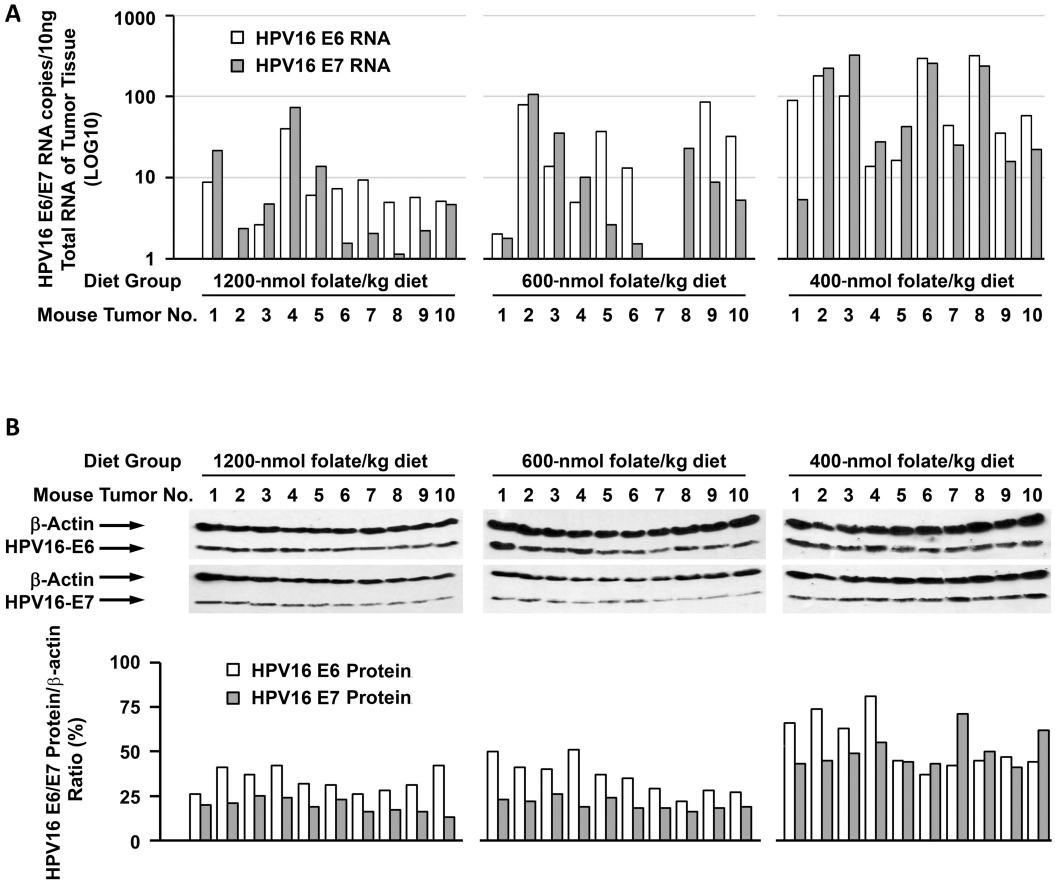
A
HPV16 E6/E7 RNA copies/10ng Total RNA of Tumor Tissue (LOG10)
1000
100
10
1
HPV16 E6 RNA
HPV16 E7 RNA
Diet Group
1200-nmol folate/kg diet
600-nmol folate/kg diet
400-nmol folate/kg diet
Mouse Tumor No. 1 2 3 4 5 6 7 8 9 10
B
Diet Group
1200-nmol folate/kg diet
600-nmol folate/kg diet
400-nmol folate/kg diet
Mouse Tumor No. 1 2 3 4 5 6 7 8 9 10
β-Actin
HPV16-E6
β-Actin
HPV16-E7
HPV16 E6/E7 Protein/β-actin Ratio (%)
100
75
50
25
0
HPV16 E6 Protein
HPV16 E7 Protein

Figure 4

ONLINE SUPPORTING MATERIAL

Folate deficiency facilitates genomic integration of Human Papillomavirus type 16 (HPV16) DNA *in vivo* in a novel mouse model for rapid oncogenic transformation of human keratinocytes

Suhong Xiao*, Ying-Sheng Tang*, Praveen Kusumanchi*‡, Sally P. Stabler[Ψ], Ying Zhang[¶], and Aśok C. Antony*‡

From *Department of Medicine, Indiana University School of Medicine, Indianapolis, Indiana 46202; Department of Medicine, [Ψ]University of Colorado Anschutz Medical Campus, Aurora, Colorado 80045; [¶]Department of Biostatistics, Indiana University Fairbanks School of Public Health, Indianapolis, Indiana 46202; [‡]Richard L. Roudebush Veterans Affairs Medical Center, Indianapolis, Indiana 46202.

SUPPLEMENTAL METHODS

Culture of (HPV16)BC-1-Ep/SL keratinocytes in high-folate F-medium and adaptation to low-folate F-medium in the absence of feeder layers. (HPV16)BC-1-Ep/SL cells were grown in F-medium that was composed of 1 part of Dulbecco's Modified Eagles Medium (DMEM) and 3 parts of Ham's F-12 medium (HyQ DME/High Glucose, and HyQ Ham's F-12), respectively (HyClone, Logan, UT), and supplemented with the following components: 10% fetal bovine serum (FBS), adenine (24-μg/mL), cholera toxin (8.4-ng/mL), epidermal growth factor (10-ng/mL), hydrocortisone (0.4-μg/mL), and insulin (5-μg/mL) (1). This medium is referred to as *high-folate* F-medium (F-HF) that contained a final folate concentration of 4.5-μM pteroylglutamic acid *plus* 13.6-nM 5-methyltetrahydrofolate; these cells are referred to hereafter as (HPV16)BC-1-Ep/SL-HF cells. Another aliquot of these cells were abruptly transferred to physiological *low-folate* F-medium (F-LF), which was similar in all other respects to supplemented F-HF except that it contained a final low-folate concentration of only 13.6-nM 5-methyltetrahydrofolate that was contributed from 10% FBS; these cells are referred to hereafter as (HPV16)BC-1-Ep/SL-LF cells. There was no difference in doubling-time between (HPV16)BC-1-Ep/SL cells stably propagated in either F-LF (29.5 h) or F-HF (30 h) (2). NIH/3T3 cells that were used as feeder layers in organotypic raft culture were also adapted to stable growth over 12 weeks in high-folate DMEM containing 10% FBS (DMEM-HF), or low-folate DMEM in which the only folate came from 10% FBS (DMEM-LF), respectively.

HPV16-organotypic raft cultures. To construct HPV16-organotypic rafts, 1-mL of a collagen premix [composed of rat tail type I collagen, 1.81-mg/mL (BD Biosciences), 0.12 N NaOH, 5% FBS, in F-12 media], was used to coat 3-micron pore size inserts (Corning BioCoat™, BD Biosciences, Bedford, MA) in 6-well plates for 5 min. Another aliquot of collagen premix (3 mL each) was impregnated with DMEM-HF- or DMEM-LF-adapted NIH/3T3 (4.5 x 10^5 cells/ml) and plated on the collagen-coated inserts. The collagen raft was allowed to contract in DMEM-HF or DMEM-LF media for 5 days at 37°C in a continuous CO_2 (5%) incubator. Then 50-μL of 1.4 x 10^7 cells/mL (7 x 10^5 cells) of either (HPV16)BC-1-Ep/SL-HF or (HPV16)BC-1-Ep/SL-LF cells were plated onto the collagen raft with *keratinocyte plating media* [F-HF or F-LF media (Ca^{2+} 0.66 mM) containing 0.5% FBS, insulin (5-μg/mL), cholera toxin (8.4-ng/mL), adenine (24-μg/mL), and hydrocortisone (0.4-μg/mL), respectively]. Four days after plating the keratinocytes, the inserts containing rafts were placed onto two 1x1-inch cotton pads (VWR Scientific, PA) on the risers of each outer well of 6-well organogenesis plates (BD BioCoat™ Deep Well Plate [6-well Plate], BD Biosciences, Bedford, MA) in order to lift to the air-liquid interface. The rafts were fed from below the insert every other day with *cornification media* composed of either F-HF or F-LF media containing 1.88-mM Ca^{2+} supplemented with 10% FBS, insulin (5-μg/mL), cholera toxin (8.4-ng/mL), adenine (24-μg/ml), hydrocortisone (0.4-μg/ml) and 10-μM 1,2-Dioctanoyl-*sn*-glycerol (C8:0) to induce a productive HPV life cycle (3). Fifteen days after being lifted to the air-liquid interface, one part of the rafts were fixed in 4% formalin, embedded in 2% agar in 1% formalin followed by paraffin, while the rest of the rafts were used to purify DNA for integration analysis.

Quantitative PCR (qPCR) for HPV16 viral load and estimation of HPV16 DNA integration ratio. HPV16 plasmid DNA was used to develop standard curves for all PCR experiments. To prepare HPV16-

organotypic raft total DNA for analysis of the HPV16 viral load by qPCR, four 18-day old HF-rafts as well as four LF-rafts were separately ground in 5-mL Dulbecco's phosphate buffered saline (D-PBS) with autoclaved sea sand (EMD Chemicals Inc, Gibbstown, NJ) using a mortar and pestle (Fisher Scientific). The resulting paste was clarified by centrifugation for 10 min at 4000 rpm in a refrigerated Beckman GPR centrifuge. After discarding the pellets, raft total DNA (including genomic and viral DNA) was extracted from the suspension using the NucleoSpin® Blood kit (Macherey-Nagel GmbH & Co., Germany). Briefly, the supernatant was incubated at 70°C for 15 min in lysis buffer containing proteinase K, and after binding to the silica column, and washing, the DNA was eluted in 100-µL elution buffer. The DNA was stored at -20°C until analysis by qPCR.

DNA copy numbers of HPV16 E6, E7, E2, and glyceraldehyde-3-phosphate dehydrogenase (GAPDH) in 50-ng raft total DNA were measured by qPCR in triplicate using the Platinum Quantitative PCR SuperMix-UDG kit (Invitrogen) and the ABI 7900 HT detection system (Applied Biosystems). Sequence-specific primers for GAPDH, HPV16 E6 and E7 were designed using the Invitrogen customer primer design online system; [these sequences are detailed in the *Supplemental Methods* of Supplemental Reference (2)].

The oligonucleotide primers used in the measurement of HPV16 DNA integration into genomic DNA were obtained from Integrated DNA Technologies (Coralville, IA). The assay for integration evaluated the ratio between HPV16 E2 and E6 DNA (4). An altered HPV16 E2/E6 ratio is an established parameter that reflects integration into cellular DNA. The principle is that a unique region of the HPV16 E2 open reading frame is most often deleted during HPV16 integration. This is targeted by one set of PCR primers and a probe, and another set targets the HPV16 E6 open reading frame. In episomal form, both targets should be equivalent, while in integrated forms, the copy numbers of HPV16 E2 would be less than those of E6. The primers for HPV16 E2 were as follows: Probe: 5'-6-FAM/CAC CCC GCC /ZEN/ GCG ACC CAT A/3IABkFQ/-3'; forward primer: 5'-AAC GAA GTA TCC TCT CCT GAA ATT ATT AG-3'; and reverse primer: 5'-CCA AGG CGA CGG CTT TG-3'. (6-FAM is 6-carboxyfluorescein; ZEN, an internal quencher 9 bases from the 5' fluorophore, is an undisclosed proprietary agent; and IABkFQ is Dark Quencher Iowa Black® FQ). The primers for HPV16 E6 were as follows. Probe: 5'-6-FAM/ CAG GAG CGA /ZEN/ CCC AGA AAG TTA CCA CAG T/3IABkFQ/-3'; forward primer: 5'-GAG AAC TGC AAT GTT TCA GGA CC-3'; and reverse primer: 5'-TGT ATA GTT GTT TGC AGC TCT GTG C-3'. The probe to primer ratio in these experiments was 1:2.

Standard curves of HPV16 E6, E7, and E2 were generated for measurement of viral DNA copies, and standard curves of GAPDH were generated for normalizing the input DNA content. Briefly, standard curves were generated using 10-fold dilutions of HPV16 plasmid or amplified GAPDH DNA (from 10^1 to 10^7 copies). Amplifications were carried out using the ABI HT7900 sequence detection system; the cycle conditions for qPCR were 50°C for 2 min, 95°C for 2 min, followed by 40 cycles of 95°C for 15 sec and 60°C for 60 sec. The actual copy numbers of HPV16 E6, E7, E2, and GAPDH were determined by qPCR using 50-ng raft total DNA, and were then normalized by the copy numbers of GAPDH.

The viral load was calculated by dividing the normalized copy number of HPV16 E6 DNA by 50-ng of raft total DNA and expressed as copies of HPV16 E6 DNA per ng raft total DNA, according to the formula by Carcopino et al (5), with the exception that we used the 'ng of raft total DNA' in place of 'cells' in that formula. An established method to determine the extent of genomic integration of HPV16 exploits the fact that only HPV16 E2 gene is disrupted upon integration into cellular DNA while HPV16 E6 remains intact (2). The amount of integrated HPV16 E6 DNA was calculated by subtracting the copy number of HPV16 E2 episomal DNA from the total copy number of HPV16 E6 DNA (episomal and integrated). The percentage of HPV16 DNA that was integrated into genomic DNA was then determined by dividing the integrated HPV16 E6 DNA copy number by total HPV16 E6 DNA copy number, and the result multiplied by 100.

Sedation and anesthesia of mice. For pre-emptive management of post-surgical discomfort, prior to surgery, mice were injected subcutaneously with 0.1 mg/kg of buprenorphine. Mice were then placed in the anesthetic induction chamber and treated with 4% isoflurane at a rate of 0.8-1L/min (Harvard Apparatus, Holliston, MA) until completely unresponsive. The mice were then moved to a sterile-draped circulating water heating pad and positioned sternally in the anesthetic nose-cone with 2% isoflurane at 0.5 L/min. A toe pinch was used to confirm unresponsiveness. Once mice were secured in the nose cone,

their eyes were lubricated with artificial tears to maintain moisture throughout the procedure. The mice were gently positioned in sternal (ventral) recumbency for surgery. The flank was disinfected with three alternating swabs of Povidone-iodine, 7.5% (0.75% available iodine) and 70% alcohol prior to surgery.

Measurement of serum homocysteine in mice. Mouse serum was measured by stable isotope dilution gas chromatography-mass spectrometry (6, 7). One of the authors (SPS) who carried out these studies was blinded to sample identity in these studies by the use of coded samples.

SUPPLEMENTAL DISCUSSION

Transformation of implanted HPV16-organotypic rafts into cancer in Beige Nude XID mice. The successful propagation of (HPV16)BC-1-Ep/SL cells as monolayers *in vitro* (1) requires a cocktail of several supplemental growth factors (in addition to the growth promoting factors found in 10% fetal bovine serum). Thus, propagation of (HPV16)BC-1-Ep/SL cells require epidermal growth factor, insulin, hydrocortisone (8), adenine (9, 10) and cholera toxin (11). Such strong dependency on growth factors is shared among other difficult-to-propagate normal [non-malignant] cells *in vitro*, such as limbic stem cells that are responsible for self-renewal of the cornea (12).

The immortalized (HPV16)BC-1-Ep/SL cells we used were obtained from Professor Lambert, University of Wisconsin (1, 13), who had documented that this is not an intrinsic tumor forming cell line; these cells are diploid with only a single karyotypic abnormality involving a duplication in the small arm of chromosome 8; and both p53 and Rb are wild type (1). Consistent with these findings, we determined that after harvesting of cultured (HPV16)BC-1-Ep/SL cells (from monolayers) and implantation of 3 million (HPV16)BC-1-Ep/SL cells into the flanks of Beige Nude XID mice, none of the 3 mice developed tumors despite observation over 9 months. This is in stark contrast to other intrinsically malignant cells, such as HeLa cells, which do not require added stimulation by more growth factors beyond that found in standard cell culture media containing 10% fetal bovine serum, and which consistently display characteristics of aggressive tumors within 2 weeks of implantation in the flanks of even less immunodeficient Athymic Nude mice (14). However, when (HPV16)BC-1-Ep/SL cells were differentiated into 3-Dimensional HPV16-organotypic rafts and implanted into several Beige Nude XID mice, *every single one of our* HPV16-organotypic raft implants in Beige Nude XID mice (that were fed either a high-folate or low-folate diet) was consistently transformed into an aggressive cancer. Such findings invariably continue to raise questions as to whether this cell line could have somehow become transformed in our hands? However, there are several additional lines of evidence against this possibility:

We determined that *(i),* these (HPV16)BC-1-Ep/SL cells can be consistently induced to <u>differentiate</u> into [3-Dimensional] HPV16-organotypic rafts that are <u>fully functional</u> in that they generate abundant numbers of complete HPV16 virus particles (2), which is ***<u>not</u>*** a feature of cancer. *(<u>ii</u>),* [As noted above], the *3-Dimensional structure* of HPV16-organotypic rafts, which actively nurtures the HPV16-life cycle *in vitro* (2), was <u>critical</u> to the development of tumors after implantation in immunodeficient mice. *(iii),* In LF-rafts implanted in folate-replete mice (Supplemental Figure 3), each malignancy developed at markedly different times (originating as early as 7 weeks and as late as 31 weeks after implantation), and each tumor had different growth rates. These are ***<u>not</u>*** characteristics of tumors arising from a clone of intrinsically malignant (HPV16)BC-1-Ep/SL cells (1, 13). *(iv),* The fact that each tumor had distinctly different patterns of integration of HPV16 DNA into genomic DNA (Supplemental Tables 6 and 7) also suggests that each tumor did not arise from the same clone.

Therefore collectively, these issues strongly argue against our (HPV16)BC-1-Ep/SL cells (1, 13) being a spontaneous tumorigenic cell line.

Cysts, dose-dense infection, and 'field cancerization'. Following implantation of HF-rafts in Beige Nude XID mice, we often noted a small subcutaneous cyst that developed within a few weeks and remained static or even partially or completely resolved before the explosive development of cancer. Although we did not analyze the content of these cysts, Brandsma et al (15), who similarly placed a fragment of HPV16-infected human foreskin under the skin of immunodeficient SCID mice and noted warty growths at 8 weeks, observed such cysts teeming with infectious HPV16 viruses. Our studies now raise the question as to whether Brandsma et al (15) could have also observed a transformation of these tissues to

cancer if they had waited longer (perhaps beyond 12 weeks). And since our mice are more immunodeficient that SCID mice, two additional questions are raised: Can HPV16-infected human foreskins also be transformed to cancer if implanted in Beige Nude XID mice under the influence of chronic or even transient folate deficiency? Conversely, can our HPV16-organotypic rafts be transformed to cancer in less immunodeficient [and less expensive] SCID or Athymic Nude mice? Exploring such models would allow for more detailed study of the stepwise transformation of primarily infected normal tissues to cancer within the context of defective immunity such as in HIV/AIDS.

Significance of global folate and vitamin-B_{12} nutrition, the HPV16-life cycle, and HPV16-induced cancer. Folate deficiency is common and 90% of women in developing countries do not receive sufficient dietary folate during pregnancy (16) which places further demands on already meager stores. Despite mandatory food fortification of folate (17) and the advent of effective HPV16 vaccines to prevent HPV16 infection and its sequelae, because high-risk HPV-induced carcinogenesis often takes over 1-2 decades to manifest in an otherwise immunocompetent general population, it would be unreasonable to expect food-fortification of folate over the past 16-18 years to meaningfully lead to any reduction in HPV-associated malignancies (in this population); *this is because HPV16 viral integration into the cellular genome may have already taken place earlier*. Moreover, the stark reality is that the vast majority of the world's women at risk (for the combination of immunosuppression due to HIV, HPV16 infection, and folate deficiency) do not have access to folate-fortified foods or to HPV vaccines (18, 19).

These issues are also relevant to vitamin-B_{12} nutrition because vitamin-B_{12} deficiency leads to a functional intracellular folate deficiency and is widespread in developing countries (among 50-75% of women in the childbearing age) where consumption of animal source foods (the main source of vitamin-B_{12}) is poor (20-25). Moreover, up to 30% of the elderly in the USA may have subclinical vitamin-B_{12} deficiency (17, 26, 27); so this population is also at risk for HPV16-induced cancers (vulvar, vaginal, cervical, penile, anal, esophageal). While not directly studied, our data (in Figure 1 B), which demonstrated that early folate deficiency can allow for genomic HPV16 integration in HPV16-harboring cells, raises the possibility that subclinical vitamin-B_{12} deficiency could likewise be permissive for early HPV16 viral integration into cellular DNA (2). Moreover, this population will not experience beneficial effects from folate-fortified foods—since they respond *only* to vitamin-B_{12} replacement. Because folate and/or vitamin-B_{12} deficiency can trigger RNA-protein events involving homocysteinylated-hnRNP-E1 and HPV16 RNA *and* lead to genomic instability (2, 28-33), understanding post-transcriptional regulation of HPV16 gene expression within the context of folate-and-vitamin-B_{12} nutrition *in vivo* is an important area for study—particularly given the high worldwide prevalence of folate- and vitamin-B_{12}- deficiency in HIV-immunosuppressed *and* HPV16-infected women who suffer from food-insecurity.

Significance of this animal model to study the HPV16 life cycle and cancer. Currently, apart from our model, there are <u>*no*</u> other comparable animal models in the HPV literature wherein HPV16-infected <u>*non-malignant tissue*</u> of <u>human</u> origin is converted so rapidly into a cancer (2). Our HPV16-organotypic rafts implanted in folate-replete and folate-deficient Beige Nude XID mice appear to mimic the human condition where aggressive HPV16-lesions such as ocular surface squamous epithelial neoplasia (34, 35) or the explosive development of cancer of the cervix can be observed in women with advanced HIV infection and AIDS (36, 37). Moreover, because there are tens of thousands of such women with food insecurity that predisposes to transient or chronic folate- or vitamin-B_{12}- deficiency, there is need for a reliable animal model that can provide insights into the natural history of HPV16-induced cancer under experimental conditions that simulate this clinical scenario. Therefore, improved understanding of the process of carcinogenesis in this animal model—*particularly with regard to early events within HPV16-organotypic rafts <u>before</u> the cancer develops*—can allow for evaluation of newer anti-HPV16 drugs (38, 39), and provide insights into innovative ways to either prevent or delay HPV16-infected tissue from developing into cancer.

DYETS #517834‡

INGREDIENT	Grams/Kg
L-Alanine	3.5
L-Arginine (free base)	11.2
L-Asparagine.H_2O	6.82
L-Aspartic Acid	3.5
L-Cystine	3.5
L-Glutamic Acid	35.0
Glycine	23.3
L-Histidine (free base)	3.3
L-Isoleucine	8.2
L-Leucine	11.1
L-Lysine HCl	18.0
L-Methionine	8.2
L-Phenylalanine	11.6
L-Proline	3.5
L-Serine	3.5
L-Threonine	8.2
L-Tryptophan	1.74
L-Tyrosine	3.5
L-Valine	8.2
Total Amino Acids	175.86
Dextrin	397.0
Sucrose	196.511
Cellulose	50.0
Corn Oil (Stab. 0.15% BHT)	100.0
Salt Mineral Mix #210020*	50.0
Vitamin Mix #317759 (Folate Free)**	10.0
Choline Chloride	2.0
Sodium Acetate	8.1
Succinyl Sulfathiazole	10.0
Folic Acid/Sucrose Mix (1 mg/g)	**0.529**

‡ Data on the formula for Dyets #517834 was provided by Dyets, Bethlehem, PA.
* Described in detail in Supplemental Table 4 (DYETS #210020)
** Described in detail in Supplemental Table 5 (DYETS #317759)

SUPPLEMENTAL TABLE 1. Modified DYETS Version of the Clifford/Koury Folate Deficient L-Amino Acid Rodent Diet [Supplemental Reference (40)] with 1% Succinyl Sulfathiazole with 0.529 mg/Kg Folic Acid.

DYETS #517833‡

INGREDIENT	Grams/Kg
L-Alanine	3.5
L-Arginine (free base)	11.2
L-Asparagine.H_2O	6.82
L-Aspartic Acid	3.5
L-Cystine	3.5
L-Glutamic Acid	35.0
Glycine	23.3
L-Histidine (free base)	3.3
L-Isoleucine	8.2
L-Leucine	11.1
L-Lysine HCl	18.0
L-Methionine	8.2
L-Phenylalanine	11.6
L-Proline	3.5
L-Serine	3.5
L-Threonine	8.2
L-Tryptophan	1.74
L-Tyrosine	3.5
L-Valine	8.2
Total Amino Acids	175.86
Dextrin	397.0
Sucrose	196.775
Cellulose	50.0
Corn Oil (Stab. 0.15% BHT)	100.0
Salt Mineral Mix #210020*	50.0
Vitamin Mix #317759 (Folate Free)**	10.0
Choline Chloride	2.0
Sodium Acetate	8.1
Succinyl Sulfathiazole	10.0
Folic Acid/Sucrose Mix (1 mg/g)	**0.265**

‡ Data on the formula for Dyets #517834 was provided by Dyets, Bethlehem, PA.
* Described in detail in Supplemental Table 4 (DYETS #210020)
** Described in detail in Supplemental Table 5 (DYETS #317759)

SUPPLEMENTAL TABLE 2. Modified DYETS Version of the Clifford/Koury Folate Deficient L-Amino Acid Rodent Diet [Supplemental Reference (40)] with 1% Succinyl Sulfathiazole with 0.265 mg/Kg Folic Acid.

DYETS #517832 ‡

INGREDIENT	Grams/Kg
L-Alanine	3.5
L-Arginine (free base)	11.2
L-Asparagine.H_2O	6.82
L-Aspartic Acid	3.5
L-Cystine	3.5
L-Glutamic Acid	35.0
Glycine	23.3
L-Histidine (free base)	3.3
L-Isoleucine	8.2
L-Leucine	11.1
L-Lysine HCl	18.0
L-Methionine	8.2
L-Phenylalanine	11.6
L-Proline	3.5
L-Serine	3.5
L-Threonine	8.2
L-Tryptophan	1.74
L-Tyrosine	3.5
L-Valine	8.2
Total Amino Acids	175.86
Dextrin	397.0
Sucrose	196.863
Cellulose	50.0
Corn Oil (Stab. 0.15% BHT)	100.0
Salt Mineral Mix #210020*	50.0
Vitamin Mix #317759 (Folate Free)**	10.0
Choline Chloride	2.0
Sodium Acetate	8.1
Succinyl Sulfathiazole	10.0
Folic Acid/Sucrose Mix (1 mg/g)	**0.177**

‡ Data on the formula for Dyets #517832 was provided by Dyets, Bethlehem, PA.
* Described in detail in Supplemental Table 4 (DYETS #210020)
** Described in detail in Supplemental Table 5 (DYETS #317759)

SUPPLEMENTAL TABLE 3. Modified DYETS Version of the Clifford/Koury Folate Deficient L-Amino Acid Rodent Diet [Supplemental Reference (40)] with 1% Succinyl Sulfathiazole with 0.265 mg/Kg Folic Acid.

DYETS #210020 ‡

INGREDIENT	grams/Kg
Calcium Carbonate	292.0
Calcium Phosphate, dibasic	3.4
Sodium Chloride	247.37
Potassium Phosphate, dibasic	343.24
Magnesium Sulfate, anhydrous	49.03
Magnesium Sulfate, monohydrate	3.64
Ferric Citrate, U.S.P.	12.52
Zinc Carbonate, basic	1.15
Cupric Carbonate, basic	1.08
Potassium Iodide/Sucrose Premix*	0.77
Sodium Selenite/Sucrose Premix**	0.99
Molybdic Acid, Ammonium Salt/Sucrose Premix***	2.5
Chromium Potassium Sulfate, Dodecahydrate	0.38
Sodium Fluoride	0.05
Sucrose, finely powdered	41.88

‡ Data on the formula for Dyets #210020 was provided by Dyets, Bethlehem, PA.
* 6.5 mg potassium iodide/g of premix
** 10.0 mg sodium selenite/g of premix
*** 10.0 mg molybdic acid, ammonium salt/g premix

SUPPLEMENTAL TABLE 4. Mineral Mix for Folate Deficient Diets used at 50 g/Kg of Diet.

DYETS #317759 ‡

INGREDIENT	grams/Kg
Thiamine HCl	0.6
Riboflavin	0.7
Pyridoxine HCl	0.7
Nicotinic Acid	3.0
Calcium Pantothenate	1.6
Folic Acid	**0.0**
Biotin	0.02
Vitamin B_{12} (0.1%)	5.0
Vitamin A Palmitate (500,000 IU/g)	0.8
Vitamin D_3 (400,000 IU/g)	0.25
Vitamin E Acetate (500 IU/g)	10.0
Menadione Sodium Bisulfite	5.0
Sucrose, finely powdered	972.33
	1000.00

‡ Data on the formula for Dyets #317759 was provided by Dyets, Bethlehem, PA.

SUPPLEMENTAL TABLE 5. Folate Deficient Vitamin Mix (Clifford Folate Deficient Vitamin Mix [Supplemental Reference (40)]) used at 10 g/Kg of Diet.

Diet Group*	Tumor sample	Number of Integration Sites†	Primers Used to Identify the Integration Site in Genomic DNA ‡
1200-nmol folate/kg diet	1	2	0841_DJ4, 2548_DJ6
	2	2	3576_DJ1, 4426_DJ1
	3	4	0892_DJ1, 2548_DJ5, 3719_DJ1, 4749_DJ1
	4	3	1509_DJ1, 3719_DJ2, 4977_DJ2
	5	4	2349_DJ1, 2548_DJ2, 3966_DJ1, 4793_DJ1
	6	2	2548_DJ3, 4601_DJ1
	7	3	0841_DJ3, 2319_DJ2, 4793_DJ3
	8	4	0940_DJ1, 1509_DJ1, 2317_DJ1, 4749_DJ3
	9	3	0018_DJ1, 3576_DJ1, 4977_DJ2
	10	2	1686_DJ1, 4426_DJ1
	Average Number of Integration Sites is 2.90 ±0.88 SD (*n* = 10) [a]		
600-nmol folate/kg diet	1	5	0892_DJ1, 2319_DJ2, 2548_DJ2, 4024_DJ2,
	2	5	0892_DJ2, 2319_DJ3, 2548_DJ4, 3576_DJ1, 4046_DJ1
	3	4	2319_DJ2, 3576_DJ1, 4793_DJ1, 5066_DJ1
	4	6	1875_DJ1, 2548_DJ2, 2882_DJ1, 4046_DJ1, 4749_DJ1, 5066_DJ1
	5	4	0018_DJ1, 1686_DJ1, 2548_DJ1, 3719_DJ2,
	6	6	0841_DJ4, 1686_DJ1, 2085_DJ2, 2317_DJ1, 3576_DJ1, 4046_DJ1
	7	4	0186_DJ2, 0892_DJ2, 2317_DJ1, 4024_DJ2
	8	4	1509_DJ2, 2319_DJ2, 3576_DJ1, 5066_DJ1
	9	6	0940_DJ1, 2317_DJ1, 2319_DJ2, 3576_DJ1, 4749_DJ1, 5066_DJ1
	10	5	0841_DJ5, 1907_DJ1, 2548_DJ4, 2967_DJ1, 4793_DJ1
	11	5	0841_DJ4, 1875_DJ1, 2548_DJ4, 2882_DJ1, 4601_DJ1
	12	4	2548_DJ4, 2967_DJ1, 3966_DJ1, 4601_DJ1
	Average Number of Integration Sites is 4.83 ±0.88 SD (*n* = 12) [b]		
400-nmol folate/kg diet	1	6	0186_DJ2, 0892_DJ2, 2319_DJ2, 2548_DJ2, 2548_DJ3, 4046_DJ1,
	2	8	0018_DJ1, 0892_DJ1, 2319_DJ2, 2548_DJ3, 2882_DJ1, 3256_DJ3, 4046_DJ1, 4426_DJ1
	3	5	0841_DJ5, 1686_DJ1, 2319_DJ3, 3966_DJ1, 4749_DJ2
	4	6	0182_DJ1, 1686_DJ1, 2548_DJ3, 2548_DJ5, 3719_DJ1, 5066_DJ1
	5	5	0186_DJ2, 0841_DJ3, 2319_DJ3, 2967_DJ1, 4046_DJ1
	6	5	0892_DJ1, 2548_DJ3, 4749_DJ1, 4793_DJ1, 5066_DJ2
	7	6	0841_DJ3, 0892_DJ2, 2548_DJ4, 2707_DJ1, 4749_DJ2, 5189_DJ2
	8	6	0892_DJ1, 2317_DJ2, 2319_DJ2, 2592_DJ1, 3576_DJ1, 4426_DJ1
	9	7	0892_DJ2, 2319_DJ1, 2548_DJ1, 3427_DJ1, 3966_DJ1, 4749_DJ1, 4793_DJ1
	10	5	0186_DJ1, 0841_DJ4, 3576_DJ1, 3719_DJ1, 5066_DJ1
	Average Number of Integration Sites is 5.90 ±0.99 SD (*n* = 10) [b]		

† The results on Average Number of Integration Sites is presented as means ± SDs, *n* = sample number as indicated. Labeled means without a common superscript letter differ, $P < 0.05$.

‡ The integration sites in various tumor samples were detected using primer pairs that can detect up to 75 validated HPV16 integrated sites [shown in Supplemental Table S7 of Supplemental Reference (41)].

SUPPLEMENTAL TABLE 6. Identification of several HPV16 DNA integration sites in the cellular genome of HPV16-*high folate*-organotypic raft (HF-raft)-derived tumors by multiplex Junction-PCR after *HF*-Rafts were implanted in Beige Nude XID Mice that were chronically fed *either* a folate-replete diet composed of 1200-nmol folate/kg diet *or* a progressively folate deficient diet composed of either 600- or 400-nmol folate/kg diet, respectively for 2 months prior to raft-implantation and until their sacrifice several weeks later (between 8-16 weeks). The integration sites detected and listed in this Table (above) are linked to the same integration sites shown in Supplemental Table 7 of Supplemental Reference (41). Data on viral-genomic DNA junctions in *RED font* indicate HPV16 insertion directly into cellular genes; *BLACK font* indicates insertion within 500 kb upstream of cellular genes, and *LIGHT BLUE font* indicates a site not within a known cellular gene.

Diet Group*	Tumor sample	Number of Integration Sites †	Primers Used to Identify the Integration Site in Genomic DNA ‡
1200-nmol folate/kg diet	1	5	0841_DJ3, 1907_DJ1, 2349_DJ1, 3576_DJ1, 5189_DJ1
	2	6	0940_DJ1, 2319_DJ1, 2548_DJ4, 3256_DJ3, 4749_DJ3, 4793_DJ2
	3	6	0182_DJ1, 0841_DJ2, 2548_DJ2, 3256_DJ1, 3427_DJ2, 5066_DJ1
	4	5	1509_DJ2, 1907_DJ1, 2548_DJ1, 3427_DJ1, 4046_DJ1
	5	7	0186_DJ1, 1509_DJ1, 1907_DJ1, 2349_DJ1, 2548_DJ4, 3719_DJ2, 4977_DJ2
	6	7	0841_DJ1, 1907_DJ1, 2319_DJ2, 2349_DJ1, 3987_DJ1, 4024_DJ2, 4601_DJ1
	7	5	1509_DJ2, 2319_DJ3, 2548_DJ3, 3427_DJ2, 3719_DJ1
	8	7	0841_DJ4, 0841_DJ5, 2317_DJ2, 2548_DJ4, 2882_DJ1, 3256_DJ1, 3987_DJ1
	9	5	0186_DJ2, 0940_DJ1, 2317_DJ1, 2707_DJ1, 3966_DJ1
	10	6	2319_DJ1, 2707_DJ1, 3719_DJ1, 3256_DJ1, 3576_DJ1, 5066_DJ2
	11	6	0892_DJ1, 2349_DJ1, 2548_DJ5, 3719_DJ1, 4426_DJ1, 5189_DJ1
	12	5	0182_DJ1, 0841_DJ2, 1875_DJ1, 2231_DJ1, 2319_DJ1
	13	6	0841_DJ1, 0841_DJ2, 2317_DJ2, 3256_DJ3, 3987_DJ1, 5066_DJ2
	14	6	0841_DJ5, 1875_DJ1, 2319_DJ1, 2319_DJ3, 4024_DJ2, 4793_DJ1
	15	7	0182_DJ1, 0186_DJ2, 0841_DJ5, 2317_DJ2, 3427_DJ2, 3719_DJ1, 4601_DJ1
	16	7	0018_DJ1, 0186_DJ2, 1686_DJ1, 2317_DJ2, 4601_DJ1, 4793_DJ1
	17	7	0841_DJ2, 1509_DJ1, 2317_DJ2, 3256_DJ1, 3576_DJ1, 4793_DJ3, 5066_DJ1
	18	6	0841_DJ1, 2548_DJ1, 2592_DJ1, 2707_DJ2, 3719_DJ1, 4024_DJ1
	19	7	0841_DJ4, 1686_DJ1, 2967_DJ1, 3719_DJ2, 4024_DJ2, 4793_DJ1, 5066_DJ1
	Average Number of Integration sites is 6.11 ±0.88 SD (*n* = 19)		

† The result on Average Number of Integration Sites is presented as mean ± SDs, *n* = sample number.

‡ The integration sites in various tumor samples were detected using primer pairs that can detect up to 75 validated HPV16 integrated sites [shown in Supplemental Table S7 of Supplemental Reference (41)].

SUPPLEMENTAL TABLE 7. Identification of multiple HPV16 integration sites in the cellular genome of HPV16-organotypic raft-derived tumors by multiplex Junction-PCR after *LF*-Rafts were implanted in Beige Nude XID Mice that were chronically fed a folate-replete diet (1200-nmol folate/kg diet) for 2 months prior to raft-implantation and until their sacrifice several weeks later (between 8 and 28 weeks). The integration sites detected and listed in this Table (above) are linked to the same integration sites shown in Supplemental Table 7 of Supplemental Reference (41). Data on viral-genomic DNA junctions in *RED font* indicate HPV16 insertion directly into cellular genes; *BLACK font* indicates insertion within 500 kb upstream of cellular genes, and *LIGHT BLUE font* indicates a site not within a known cellular gene.

ONLINE SUPPORTING MATERIAL

SUPPLEMENTAL FIGURES WITH LEGENDS

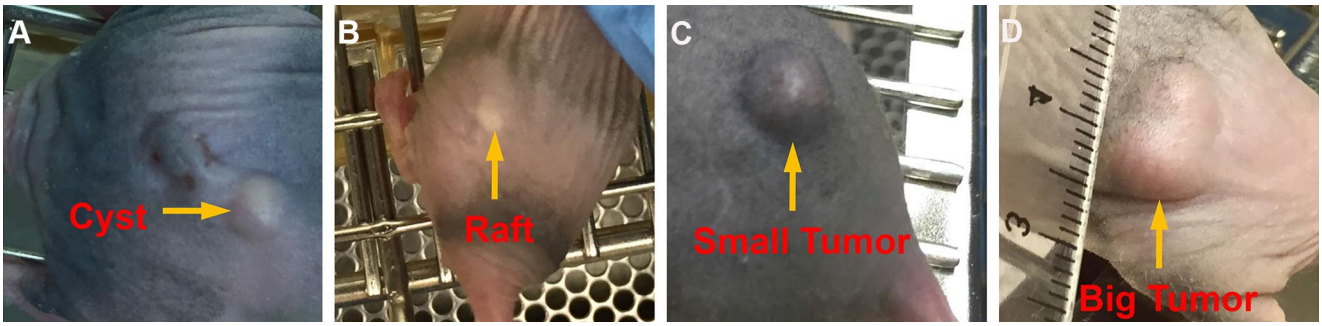

SUPPLEMENTAL FIGURE 1. Photographs that highlight changes in the skin overlying subcutaneously implanted HPV16-organotypic rafts in the flanks of Beige Nude XID Mice (*Panels* A-D).
(*Panel* A), Development of a small cyst adjacent to the subcutaneously implanted HPV16-*high folate*-organotypic raft following removal of surgical clips.
(*Panel* B), Small hypopigmented area signifying healing of skin after regression of the cyst.
(*Panel* C), Formation of a firm nodule approximating 1 cm^3 signifying the development of an early cancer arising from the implanted HF-raft.
(*Panel* D), Evidence of more rapid growth of tumor within a few days of onset of a small nodule.

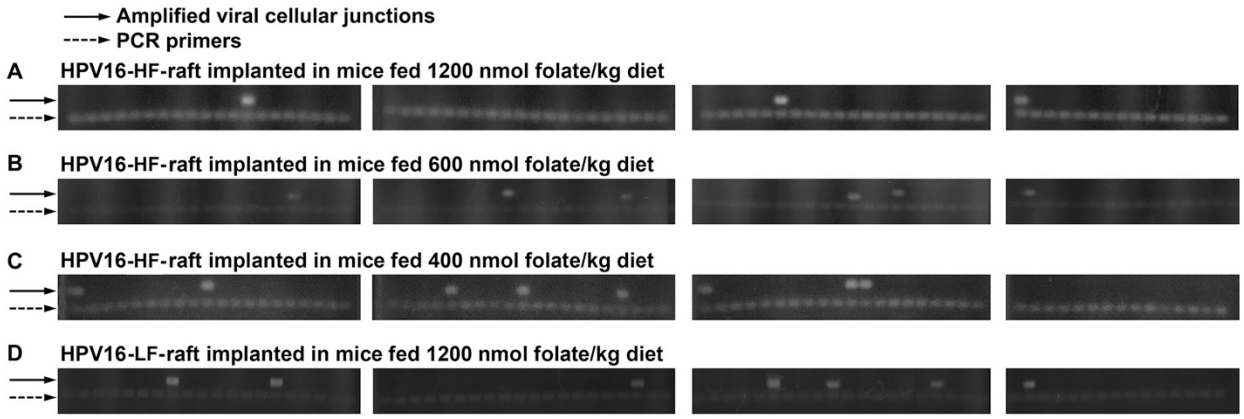

SUPPLEMENTAL FIGURE 2. PCR product analysis by Multiplex Junction-PCR to demonstrate amplified signals from unique viral-cellular junctions from representative tumors of mice that were implanted with HF-rafts and fed either a 1200-, 600- or 400-nmol folate/kg diet (*Panels* A, B, C, respectively) for 2 months prior to raft-implantation and until their sacrifice several weeks later (between 8-16 weeks). In *Panel* D, the data is from a representative tumor from mice that were fed a 1200-nmol folate/kg diet for 2 months prior to LF-raft implantation and until their sacrifice several weeks later. Each well contains one of 75 different primers and each of the slower moving (brighter) bands in these representative gels reflect amplification of these unique viral-cellular integration sites (indicated by *solid arrows*). The faster moving signals in each well are from one of 75 distinct pairs of unamplified primers (indicated by *dashed arrows*).

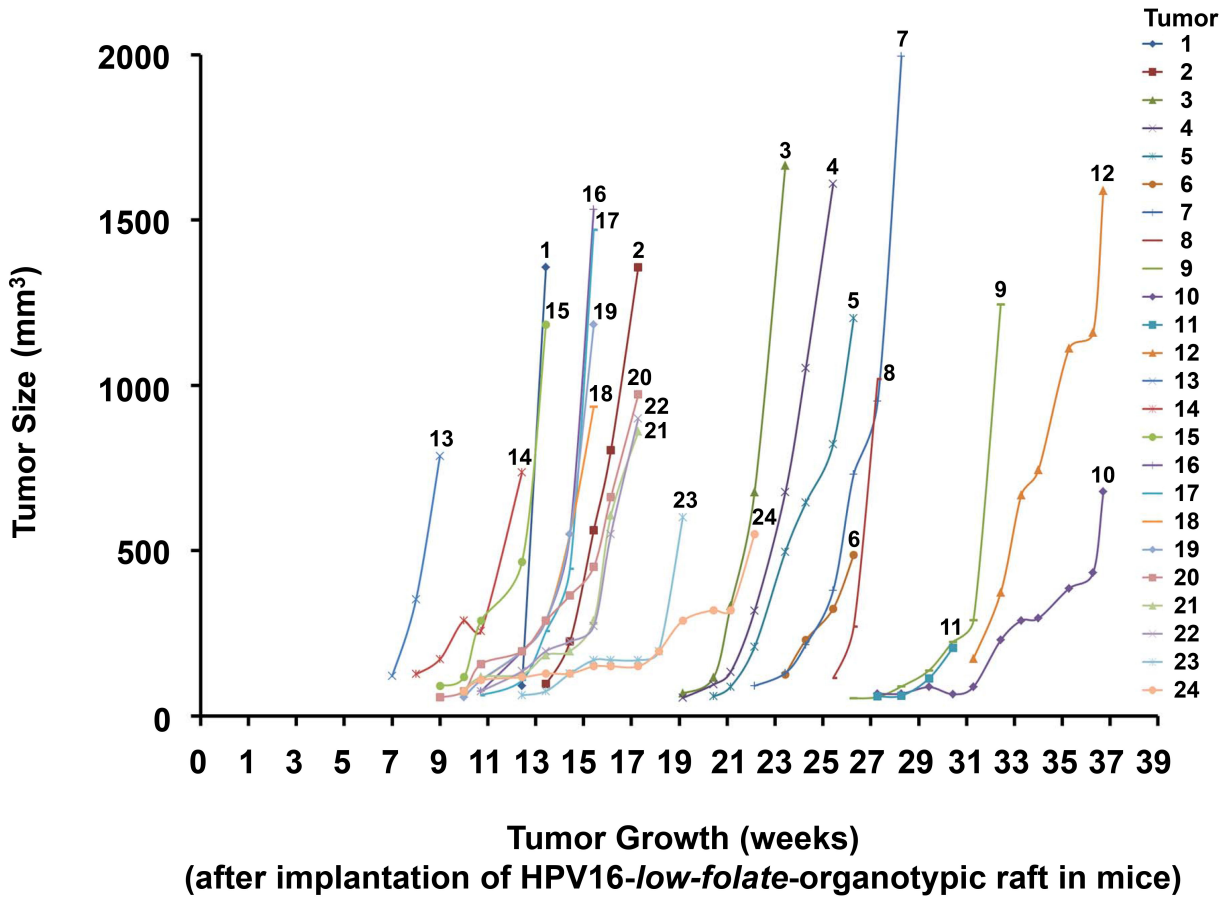

SUPPLEMENTAL FIGURE 3. Development of aggressive tumors over a longer duration after LF-rafts were implanted subcutaneously in Beige Nude XID mice that were chronically fed a folate-replete diet (1200-nmol folate/kg diet) for 2 months prior to raft-implantation and until their sacrifice several weeks later (as indicated by the tumor number). These LF-raft implantation studies were carried out in two batches: Batch 1 included tumors #1-12, and Batch 2 included tumors #13-24. A tumor number was assigned in sequence when the mouse was sacrificed; this corresponds to the color coding on the right.

ONLINE SUPPORTING MATERIAL

SUPPLEMENTAL REFERENCES

1. Flores ER, Allen-Hoffmann BL, Lee D, Sattler CA, and Lambert PF. Establishment of the human papillomavirus type 16 (HPV-16) life cycle in an immortalized human foreskin keratinocyte cell line. *Virology.* 1999;262:344-54.
2. Xiao S, Tang YS, Khan RA, Zhang Y, Kusumanchi P, Stabler SP, Jayaram HN, and Antony AC. Influence of physiologic folate deficiency on human papillomavirus type 16 (HPV16)-harboring human keratinocytes in vitro and in vivo. *J Biol Chem.* 2012;287:12559-77.
3. Genther SM, Sterling S, Duensing S, Munger K, Sattler C, and Lambert PF. Quantitative role of the human papillomavirus type 16 E5 gene during the productive stage of the viral life cycle. *J Virol.* 2003;77:2832-42.
4. Peitsaro P, Johansson B, and Syrjanen S. Integrated human papillomavirus type 16 is frequently found in cervical cancer precursors as demonstrated by a novel quantitative real-time PCR technique. *J Clin Microbiol.* 2002;40:886-91.
5. Carcopino X, Henry M, Benmoura D, Fallabregues AS, Richet H, Boubli L, and Tamalet C. Determination of HPV type 16 and 18 viral load in cervical smears of women referred to colposcopy. *J Med Virol.* 2006;78:1131-40.
6. Kolhouse JF, Stabler SP, and Allen RH. Identification and perturbation of mutant human fibroblasts based on measurements of methylmalonic acid and total homocysteine in the culture media. *Archives of Biochemistry & Biophysics.* 1993;303:355-60.
7. Tang YS, Khan RA, Xiao S, Hansen DK, Stabler SP, Kusumanchi P, Jayaram HN, and Antony AC. Evidence favoring a positive feedback loop for physiologic auto upregulation of hnRNP-E1 during prolonged folate deficiency in human placental cells. *J Nutr.* 2017;147:482-98.
8. Rheinwald JG. Serial cultivation of normal human epidermal keratinocytes. *Methods Cell Biol.* 1980;21A:229-54.
9. Allen-Hoffmann BL, and Rheinwald JG. Polycyclic aromatic hydrocarbon mutagenesis of human epidermal keratinocytes in culture. *Proc Natl Acad Sci U S A.* 1984;81:7802-6.
10. Flaxman BA, and Harper RA. In vitro analysis of the control of keratinocyte proliferation in human epidermis by physiologic and pharmacologic agents. *J Invest Dermatol.* 1975;65:52-9.
11. Okada N, Kitano Y, and Ichihara K. Effects of cholera toxin on proliferation of cultured human keratinocytes in relation to intracellular cyclic AMP levels. *J Invest Dermatol.* 1982;79:42-7.
12. Yu M, Bojic S, Figueiredo GS, Rooney P, de Havilland J, Dickinson A, Figueiredo FC, and Lako M. An important role for adenine, cholera toxin, hydrocortisone and triiodothyronine in the proliferation, self-renewal and differentiation of limbal stem cells in vitro. *Exp Eye Res.* 2016;152:113-22.
13. Flores ER, Allen-Hoffmann BL, Lee D, and Lambert PF. The human papillomavirus type 16 E7 oncogene is required for the productive stage of the viral life cycle. *J Virol.* 2000;74:6622-31.
14. Sun XL, Murphy BR, Li QJ, Gullapalli S, Mackins J, Jayaram HN, Srivastava A, and Antony AC. Transduction of folate receptor cDNA into cervical carcinoma cells using recombinant adeno-associated virions delays cell proliferation in vitro and in vivo. *J Clin Invest.* 1995;96:1535-47.
15. Brandsma JL, Brownstein DG, Xiao W, and Longley BJ. Papilloma formation in human foreskin xenografts after inoculation of human papillomavirus type 16 DNA. *J Virol.* 1995;69:2716-21.
16. Torheim LE, Ferguson EL, Penrose K, and Arimond M. Women in resource-poor settings are at risk of inadequate intakes of multiple micronutrients. *J Nutr.* 2010;140:2051S-8S.
17. Antony AC. Megaloblastic Anemias. Chapter 39. In: Hoffman R, Benz EJ (Jr), Silberstein LE, Heslop HE, Weitz JI, Anastasi J, Salama ME, Abutalib SA (eds). *Hematology: Basic Principles and Practice, Seventh Edition*. Philadelphia: Elsevier Saunders; 2017:514-45.
18. Crider KS, Bailey LB, and Berry RJ. Folic acid food fortification-its history, effect, concerns, and future directions. *Nutrients.* 2011;3:370-84.
19. Antony AC. Megaloblastic Anemias. Chapter 164. In: Goldman L, and Schafer AI eds. *Goldman-Cecil Medicine, 25th Edition*. New York: Elsevier Saunders; 2015:1104-14.
20. Antony AC. Vegetarianism and vitamin B-12 (cobalamin) deficiency. *Am J Clin Nutr.* 2003;78:3-6.

21. Pawlak R, Parrott SJ, Raj S, Cullum-Dugan D, and Lucus D. How prevalent is vitamin B(12) deficiency among vegetarians? *Nutr Rev.* 2013;71:110-7.
22. Dang S, Yan H, Zeng L, Wang Q, Li Q, Xiao S, and Fan X. The status of vitamin B12 and folate among Chinese women: a population-based cross-sectional study in northwest China. *PLoS One.* 2014;9:e112586.
23. Kapil U, and Bhadoria AS. Prevalence of Folate, Ferritin and Cobalamin Deficiencies amongst Adolescent in India. *J Family Med Prim Care.* 2014;3:247-9.
24. Koc A, Kocyigit A, Soran M, Demir N, Sevinc E, Erel O, and Mil Z. High frequency of maternal vitamin B12 deficiency as an important cause of infantile vitamin B12 deficiency in Sanliurfa province of Turkey. *Eur J Nutr.* 2006;45:291-7.
25. Antony AC. Evidence for potential underestimation of clinical folate deficiency in resource-limited countries using blood tests. *Nutrition Reviews.* 2017;75:600-15.
26. Stabler SP, and Allen RH. Vitamin B12 deficiency as a worldwide problem. *Annu Rev Nutr.* 2004;24:299-326.
27. Stabler SP. Clinical practice. Vitamin B12 deficiency. *N Engl J Med.* 2013;368:149-60.
28. Das KC, and Herbert V. In vitro DNA synthesis by megaloblastic bone marrow: effect of folates and cobalamins on thymidine incorporation and de novo thymidylate synthesis. *Am J Hematol.* 1989;31:11-20.
29. Koury MJ, Horne DW, Brown ZA, Pietenpol JA, Blount BC, Ames BN, Hard R, and Koury ST. Apoptosis of late-stage erythroblasts in megaloblastic anemia: association with DNA damage and macrocyte production. *Blood.* 1997;89:4617-23.
30. Ciappio E, and Mason JB. In: Bailey LB ed. *Folate in Health and Disease Second Edition*. Boca Raton, FL: CRC Press; 2010:235-62.
31. Ames BN, and Wakimoto P. Are vitamin and mineral deficiencies a major cancer risk? *Nat Rev Cancer.* 2002;2:694-704.
32. Duthie SJ, and Hawdon A. DNA instability (strand breakage, uracil misincorporation, and defective repair) is increased by folic acid depletion in human lymphocytes in vitro. *FASEB J.* 1998;12:1491-7.
33. Dianov GL, Timchenko TV, Sinitsina OI, Kuzminov AV, Medvedev OA, and Salganik RI. Repair of uracil residues closely spaced on the opposite strands of plasmid DNA results in double-strand break and deletion formation. *Mol Gen Genet.* 1991;225:448-52.
34. Mittal R, Rath S, and Vemuganti GK. Ocular surface squamous neoplasia - Review of etio-pathogenesis and an update on clinico-pathological diagnosis. *Saudi J Ophthalmol.* 2013;27:177-86.
35. Di Girolamo N. Association of human papilloma virus with pterygia and ocular-surface squamous neoplasia. *Eye (Lond).* 2012;26:202-11.
36. Maiman M, Fruchter RG, Guy L, Cuthill S, Levine P, and Serur E. Human immunodeficiency virus infection and invasive cervical carcinoma. *Cancer.* 1993;71:402-6.
37. Maiman M. Cervical neoplasia in women with HIV infection. *Oncology.* 1994;8:83-9.
38. Baleja JD, Cherry JJ, Liu Z, Gao H, Nicklaus MC, Voigt JH, Chen JJ, and Androphy EJ. Identification of inhibitors to papillomavirus type 16 E6 protein based on three-dimensional structures of interacting proteins. *Antiviral Res.* 2006;72:49-59.
39. Rietz A, Petrov DP, Bartolowits M, DeSmet M, Davisson VJ, and Androphy EJ. Molecular Probing of the HPV-16 E6 Protein Alpha Helix Binding Groove with Small Molecule Inhibitors. *PLoS One.* 2016;11:e0149845.
40. Bills ND, Koury MJ, Clifford AJ, and Dessypris EN. Ineffective hematopoiesis in folate-deficient mice. *Blood.* 1992;79:2273-80.
41. Xu B, Chotewutmontri S, Wolf S, Klos U, Schmitz M, Durst M, and Schwarz E. Multiplex Identification of Human Papillomavirus 16 DNA Integration Sites in Cervical Carcinomas. *PLoS One.* 2013;8:e66693.